Mon. Not. R. Astron. Soc. **308**, 233–256 (1999)

X-ray spectra of the RIXOS source sample

J. P. D. Mittaz,[1] F. J. Carrera,[1,2] E. Romero-Colmenero,[1] K. O. Mason,[1] G. Hasinger,[3] R. McMahon,[4] H. Andernach,[5] R. Bower,[6] J. Burgos-Martin,[7] J. I. González-Serrano[2] and D. Wonnacott[1]

[1]*Mullard Space Science Laboratory, University College London, Holmbury St. Mary, Dorking, Surrey RH5 6NT*
[2]*Instituto de Física de Cantabria, Consejo Superior de Investigaciones Científicas – Universidad de Cantabria, Santander, Spain*
[3]*Astrophysikalisches Institut Potsdam, An der Sternwarte 16, Potsdam, Germany*
[4]*Institute of Astronomy, Madingley Road, Cambridge*
[5]*Depto. de Astronomía, IFUG, Guanajuato, Mexico*
[6]*Department of Physics, University of Durham, South Road, Durham*
[7]*Instituto de Astrofisica de Canarias, La Laguna, Tenerife, Spain*

Accepted 1999 April 7. Received 1999 March 30; in original form 1997 April 2

ABSTRACT

We present results of an extensive study of the X-ray spectral properties of sources detected in the RIXOS survey, which is a large, nearly complete sample of objects detected serendipitously in *ROSAT* PSPC fields down to a flux limit of $3\times10^{-14}\,\mathrm{erg\,cm^{-2}\,s^{-1}}$ (0.5–2 keV). We show that for X-ray surveys containing sources with low count rate, such as RIXOS, spectral slopes estimated using simple hardness ratios in the *ROSAT* band can be biased. Instead, we analyse three-colour X-ray data using statistical techniques appropriate to the Poisson regime which remove the effects of this bias. We also show that the use of three-colour data enables some discrimination between thermal and non-thermal spectra. We have then applied this technique to the RIXOS survey to study the spectral properties of the sample.

For the AGN we find an average energy index of 1.05 ± 0.05, with no evidence for spectral evolution with redshift. Individual AGN are shown to have a range of properties, including soft X-ray excesses and intrinsic absorption. Narrow-emission-line galaxies (NELGs) also seem to fit to a power-law spectrum, which may indicate a non-thermal origin for their X-ray emission. We infer that most of the clusters in the sample have a bremsstrahlung temperature >3 keV, although some show evidence for a cooling flow. The stars deviate strongly from a power-law model but fit to a thermal model. Finally, we have analysed the whole RIXOS sample (extending the flux cut-off to the sensitivity threshold of each individual observation) containing 1762 sources to study the relationship between spectral slope and flux. We find that the mean spectral slope of the sources hardens at lower fluxes, in agreement with results from other samples. However, a study of the individual sources demonstrates that the majority have relatively soft spectra even at faint flux levels, and the hardening of the mean is caused by the appearance of a population of very hard sources at the lowest fluxes. This has implications for the nature of the soft X-ray background.

Key words: surveys – galaxies: active – quasars: general – X-rays: galaxies – X-rays: stars.

1 INTRODUCTION

X-ray surveys have proven to be powerful tools in extending our knowledge of a range of object types, from highly luminous AGN to active stars. Surveys of ‘serendipitous’ detections in the fields of view of imaging X-ray instruments, examples of which are the *Einstein* Medium Sensitivity Survey (EMSS) (Gioia et al. 1990) and the *EXOSAT* High Galactic Latitude Survey (HGLS) (Giommi et al. 1991), have provided large samples with which to make detailed statistical studies with relatively well-understood selection biases. With the advent of *ROSAT*, ever more extensive and sensitive surveys are becoming available, ranging from the *ROSAT* all-sky survey, which sampled relatively bright source populations, to deep pencil-beam surveys such as those of Hasinger et al.

(1993) and Branduardi-Raymont et al. (1994). Other samples have concentrated on serendipitous sources discovered in *ROSAT* pointed data (e.g. Boyle et al. 1994, 1995; Carballo et al. 1995).

The spectral properties of such samples can be a crucial element in understanding the nature of the X-ray emission. However, much of the work to date has considered only the broad-band fluxes of survey sources. The subject of this paper is the RIXOS survey of *ROSAT* field sources, which covers a total of 20 deg^2 of sky and has a high level of optical identification completeness (~94 per cent over a 15 deg^2 subarea) down to a flux level 3×10^{-14} erg cm^{-2} s^{-1}. This flux cut-off is set so as to bridge the gap in sensitivity and sky coverage between the *ROSAT* all-sky survey and the deepest pencil-beam *ROSAT* surveys. As the flux cut-off of RIXOS is set at a level which is much higher than the sensitivity threshold of the *ROSAT* observations used, sufficient numbers of X-ray photons have been detected from all RIXOS sources to provide some information about their overall spectral distribution. This paper examines the X-ray spectral properties of the RIXOS sample. Other aspects of the RIXOS survey are covered in Page et al. (1996), Puchnarewicz et al. (1996, 1997), Romero-Colmenero et al. (1998), Carrera et al. (1998) and Mason et al. (in preparation). The paper discussing cluster evolution by Castander et al. (1995) is based on a subset of the RIXOS complete sample.

2 THE RIXOS SAMPLE

The X-ray data are taken from the RIXOS sample of objects (Mason et al., in preparation) and have been constructed from serendipitous sources discovered in 82 pointed *ROSAT* PSPC fields. The fields were chosen to have nominal exposure times greater than 8 ks and to be above a Galactic latitude of 28°. This limit enables us to sample sources at faint fluxes without the problem of identifying them in crowded fields. From each field we have excluded the target of the observation and consider only sources at less than 17 arcmin off-axis. Such sources have the best positional certainty and are not masked by the detector window support structure. Survey sources are selected in the 0.4–2 keV band; the poorer point spread function (PSF) and increased background due to diffuse Galactic X-ray emission make the detection of X-ray sources more difficult at softer energies.

Full details of the optical imaging and spectroscopy and identification process are given in Mason et al. (in preparation). Over 82 fields (or 20.2 deg^2) our sample is completely identified down to a flux limit of 8.4×10^{-14} erg cm^{-2} s^{-1} and over 64 fields (or 14.9 deg^2) we have complete identifications down to our target flux limit of 3×10^{-14} erg cm^{-2} s^{-1}. This flux limit is well above the detection limit for all our fields, and for many sources gives a reasonable number of observed counts. Table 2 lists all the sources in the RIXOS fields above a flux limit of 3×10^{-14} erg cm^{-2} s^{-1} (0.5–2 keV), giving field ID and source ID (for details see Mason et al., in preparation) together with the Galactic column (N_H), date of observation and exposure time (column 5). This is the sample with which we are primarily concerned here, and it will be referred to here as RIXOS.

In total, the RIXOS sample contains 401 sources, of which 347 have been identified. The identification of the sources has been based largely on the optical spectra, and we have split them into six categories. These are active galactic nuclei (AGN), narrow-emission-line galaxies (NELGs, which may include Seyfert 2 galaxies, LINERs, and H II region galaxies), isolated galaxies, clusters of galaxies, active stars and dMe stars. Of the 347 identified sources, 16 are so close together that no separate spectra could be extracted for them; their spectra are included in Table 2 as ‘MERG’. Five more sources (one of them unidentified) were in fields 115 and 116 (Mason et al., in preparation), for which no public archival X-ray data were available at the time of writing. This leaves us with 327 identified sources with available X-ray data, of which 205 have been classified as AGN, 18 as NELGs, six as isolated galaxies, 30 as clusters, 46 as stars and 22 as dMe stars. In addition, we have also fitted the spectra of 56 unidentified sources (included in Table 2 as ‘UNKN’). In total, the RIXOS sample forms the largest serendipitous survey constructed from *ROSAT* PSPC pointings to date, with a larger sky coverage than comparable samples such as the Cambridge-Cambridge *ROSAT* Serendipity Survey.

3 DATA REDUCTION

From the RIXOS sample we have taken all those sources which have a firm optical identification and have extracted three-colour X-ray data. After the recommendation of Snowden et al. (1994) we have used bands S1 (channels 8–41), H1 (channels 52–90) and H2 (channels 91–201). For each field we have constructed an image in each of the three colours and have ensured the optimal signal-to-noise ratio by excluding high background times and those times when the attitude solution was bad. In general, this excluded between 5 and 20 per cent of the data. We then extracted the source counts for all the known sources in the field (including those with no identification) using an extraction circle of 54 arcsec, which includes 90 per cent of the *ROSAT* PSF and maximizes the signal-to-noise ratio for weak sources. In those cases where there was a contaminating source nearby, the extraction circles were reduced in size until there was no overlap. The sizes of the extraction circles for each source are listed in Table 2 (column 6) and the fraction of the PSF included for each source is taken into account during the spectral fitting process (Section 5.1).

As we are studying very faint sources, we have been careful to obtain an accurate estimate of the background. After masking out all the sources from an image, it was flattened using the exposure map supplied as part of the standard SASS processing. As the exposure map corrects for vignetting and other instrumental effects, we can obtain an accurate estimate of the image background corrected for systematic instrumental effects by summing over a large number of pixels. For RIXOS we summed the data between 5.2 and 10.8 arcmin off-axis, thereby excluding the residual effects of any bright central source. We can then estimate the background at any given source position from the mean background using data from the exposure map at the required position. This method yields a very accurate background estimate based on a very large number of pixels compared to the number of pixels in the source extraction circle, and to a very good degree of approximation we can then assume that this background estimate has a negligible error. Table 2 lists the the extracted counts for the RIXOS sample (columns 8–10) and the background estimates in each of the three bands (columns 11–13).

4 THE COLOUR–COLOUR DIAGRAM

As a first step in studying the spectral properties of the sources, we have constructed a colour–colour diagram including all identified sources in the RIXOS sample (Fig. 1). Our normalized colours are defined as

$$C1 = (S - H1)/(S + H1) \tag{1}$$

and

$$C2 = (H2 - H1)/(H2 + H1). \tag{2}$$

The first plot in Fig. 1 shows uncorrected colours, and the second shows colours corrected for the effect of Galactic absorbing column where applicable. As the correction for the Galactic column is model-dependent, we have used a power law fitted to the three colours (see Section 6), and have only applied the correction to extragalactic sources. Fig. 1 shows a number of features. On average, the AGN tend to be softer than most of the other sources when corrected for Galactic absorption, although it is clear that not all the AGN are soft, and some AGN occupy portions of the diagram appropriate to hard sources (see also Fig. 7). Five out of 205 AGN have $C1 < 0$, implying that they are very hard or intrinsically absorbed. A further 15 sources do not appear in this diagram at all since they were not detected in the soft band, and of these six are identified with AGN. This implies that ~5 per cent of AGN are very hard and are candidates for intrinsic absorption.

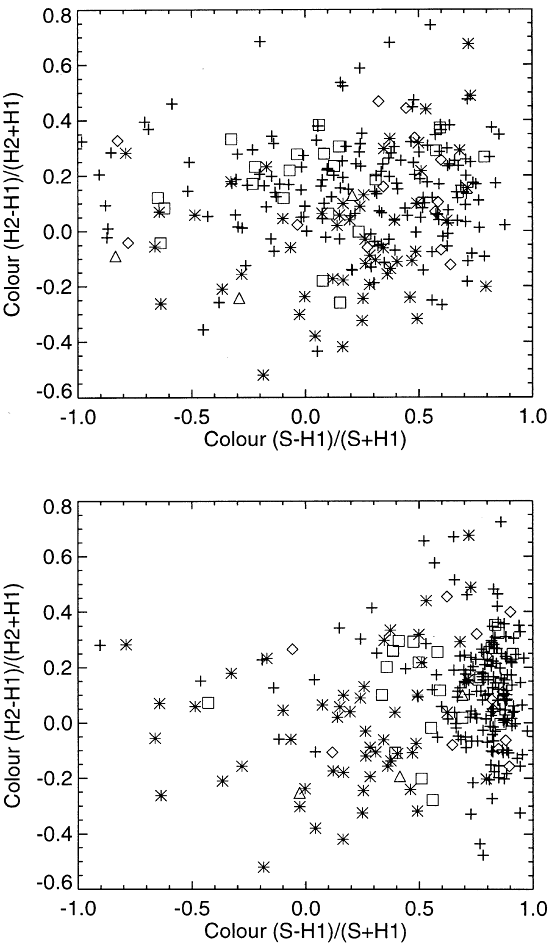

Figure 1. The colour–colour diagrams for the RIXOS sample of objects. The top panel shows the data uncorrected for the effect of Galactic N_{H}, while the bottom panel is corrected for Galactic N_{H}. Different classes of objects have different symbols [+ AGN, ◇ ELG, △ galaxies, □ clusters and * stars (including dMe stars)].

As a first step in categorizing the spectral characteristics of our sample, we have quantified the differences between the different types of X-ray sources in the colour–colour plot by using a two-dimensional Kolmogorov–Smirnov (KS) test. The method used is taken from Press et al. (1992), and the results are shown in Table 1 for both the uncorrected and corrected colour–colour data. The probabilities quoted are of the two samples being drawn from the same parent distribution. However, many of the sources are faint and therefore have large uncertainties which are not taken into account by a standard KS test. We have quantified the possible effect of the measurement uncertainties on the KS probabilities. To do this, we have simulated 100 samples with the same flux distribution as our real sample, but assuming that all sources have power-law slopes distributed in a similar way to the AGN. We have used a mean slope of $\alpha = 1$ and a dispersion of 0.55. The numbers in brackets in Table 1 are the fraction of the time that a KS probability was obtained that was smaller than the one seen in the original data set. This therefore gives an indication of the likelihood of obtaining a probability as small as that seen or better by chance alone, given our assumption concerning the distribution of AGN slopes.

The two-dimensional KS test emphasizes the fact that on average the AGN and objects classified as NELGs lie in a region of the colour–colour plot distinct from the clusters and stars. The similarity between the NELGs and the AGN, as well as the disparity between the NELGs and the clusters/stars, is intriguing and may hint at NELGs containing AGN-like activity. If the emission were to arise solely from thermal emission from hot gas, the NELGs may be expected to lie further to the left in the colour–colour diagram, closer to the clusters.

The other sources lie to the left of the AGN in the colour–colour diagram. That the stars and clusters are distinct from the AGN is not surprising, given the different physical mechanism known to underlie their X-ray emission. From Fig. 1, the stars constitute the hardest sources, with the clusters lying midway between the stars and AGN. However, within the stars from Table 1 there is a further difference which would seem to indicate that the dMe stars are softer than other active stars. Given the multi-temperature nature of the emission from stars, simple three-colour data cannot give more than an indication of a difference in the X-ray spectra between these two classes of objects.

Table 1. Two-dimensional Kolmogorov–Smirnov probabilities for the different classes of objects in the sample based on the both the uncorrected and corrected colour–colour diagram. The numbers in brackets are the associated probabilities based on simulated data sets.

Source 1 type	Source 2 type	2D KS	2D KS (corr)
AGN	ELG	0.108 (0.08)	0.246 (0.21)
AGN	Galaxy	0.005 (0.00)	0.025 (0.02)
AGN	Cluster	0.077 (0.06)	0.002 (0.00)
AGN	Star	0.000 (0.00)	0.000 (0.00)
AGN	M Star	0.004 (0.00)	0.000 (0.00)
ELG	Galaxy	0.052 (0.03)	0.115 (0.08)
ELG	Cluster	0.253 (0.17)	0.079 (0.03)
ELG	Star	0.041 (0.02)	0.000 (0.00)
ELG	M Star	0.013 (0.01)	0.001 (0.00)
Galaxy	Cluster	0.043 (0.01)	0.267 (0.17)
Galaxy	Star	0.275 (0.13)	0.268 (0.22)
Galaxy	M Star	0.020 (0.00)	0.454 (0.22)
Cluster	Star	0.006 (0.01)	0.000 (0.00)
Cluster	M Star	0.001 (0.00)	0.004 (0.00)
Star	M Star	0.057 (0.01)	0.057 (0.01)

5 MODEL FITTING

5.1 The fitting technique

A simple two-colour diagram can only provide information in a general sense about the X-ray emission of the RIXOS sample. In order to gain a deeper understanding, it is necessary to fit models. Two main approaches have been used in obtaining spectral information for similar survey data. The first is a simple hardness ratio to determine the power-law slope of low count rate data, and χ^2 fitting for sources with enough counts (e.g. Ciliegi et al. 1997). However, this approach has the twin disadvantages of not analysing the data in a uniform way and not taking into account the Poissonian nature of the data for weak sources. The other method is to sum up the spectra for sources with similar $N_{\rm H}$ and use a standard χ^2 fit to the summed data. This allows us to have reasonably high-resolution spectra, but has the disadvantage of losing all information about the individual sources within each $N_{\rm H}$ band.

We have addressed these problems by fitting two-parameter models to our three-colour data for each individual source. By using three colours, we can maximize the signal in each band while retaining one degree of freedom for the fitting process. It is also possible to take into account the Poissonian nature of the data directly, by minimizing the correct statistic. That there is a requirement to use such a statistic is clear from Fig. 2, as many of our sources have <15 counts in one or more of the three spectral bands used.

A statistic appropriate to the Poisson regime is described by Cash (1979). This has been successfully applied to the problem, among others, of source searching in both the WFC all-sky survey (Pounds et al. 1993) and the EUVE all-sky survey (Bowyer et al. 1994). For spectral fitting of low-count-rate sources a maximum-likelihood method using the Cash statistic is appropriate, instead of minimizing χ^2 as in the Gaussian regime.

The Cash statistic is derived from the probability of observing n counts for a given mean μ. In the Poisson regime this is given by

$$P = \frac{\mu^n \mathrm{e}^{-\mu}}{n!}; \tag{3}$$

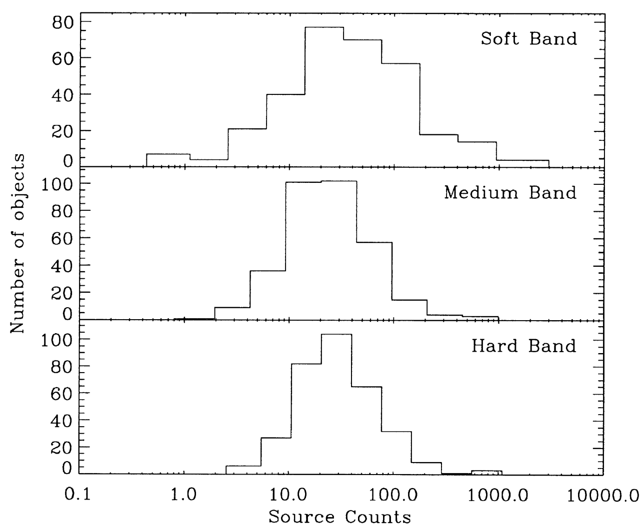

Figure 2. Total source counts in each of the three colours (soft – channels 8–41, medium – channels 52–90, hard – channels 91–201). Many of the sources are close to or at the Poisson limit.

therefore, for a distribution of counts n_i with predicted means in each bin μ_i, the total probability is given by

$$P = \prod_{i=1}^{N} \frac{\mu_i^{n_i} \mathrm{e}^{-\mu_i}}{n_i!}. \tag{4}$$

By converting this into a maximum-likelihood formulation, we then arrive at the Cash statistic

$$C = -2\log P = -2\sum_{i=1}^{N} n_i \log(\mu_i) - \mu_i - \log(n_i!). \tag{5}$$

As $\log(n!)$ is a constant, we can drop it from the calculation, since we are only interested in the minimum of C, not its absolute value.

To fit the data, we must arrive at a set of predicted values for μ_i which minimize C. To maintain the strict Poissonian nature of the data, we fit the total number of observed counts from the source and background within a circle of radius r_i in each band with a mean μ_i, i.e., we minimize

$$C' = -2\sum_{i=1}^{N} n_i \log(PSF(r_i) \times model_i(\alpha_1, \alpha_2, \alpha_3) + b_i) - [PSF(r_i) \times model_i(\alpha_1, \alpha_2, \alpha_3) + b_i], \tag{6}$$

where $model_i(\alpha_1, \alpha_2, \alpha_3)$ is the predicted total counts in band i, given some model defined by $\alpha_1, \alpha_2, \alpha_3$. $PSF(r_i)$ is the fraction of the PSF contained within a radius r_i, and b_i is the background contained within radius r_i. For the case of a power law, α_1, α_2 and α_3 would be the normalization, the power-law index and the amount of Galactic absorption respectively. Note that equation (6) assumes that the background is known to a much higher level of statistical accuracy than the source counts, so that the error on the background is negligible. For the RIXOS data, this is the case (see Section 3).

Not only does this method deal correctly with the Poissonian nature of the data, but it also enables us to obtain estimates of the spectrum when we have upper limits in one or more of the three bands. As the method fits the total observed counts (source plus background), it automatically takes into account such upper limits. This is because even in those cases where the predicted background is larger than the observed number of counts, the predicted number of source counts [i.e., $model_i(\alpha_1, \alpha_2, \alpha_3)$] will always be greater than zero. The case where no source counts are detected is then taken as a simple statistical fluctuation of the model predicted *positive* source counts.

5.2 Error estimation

Once we have found a minimum of the Cash statistic, the next step is to calculate the confidence limits on the fitted parameters. This can be done in an identical way to the procedures standardly used in χ^2 fitting, as the ΔC statistic is distributed as $\Delta\chi^2$ (Cash 1979). However, for those sources near the Poisson limit it is difficult to write down a simple number as the error on a given parameter, because the confidence contours tend to be asymmetric. Fig. 3 show examples of the confidence contours for both a source near the Poisson limit and a source with a large number of counts. In the case of a source near the Poisson limit the probability contours from a $\Delta\chi^2$ surface and a C surface are markedly different, with a tighter constraint on the power-law slope from the ΔC contours. On the other hand, in the case of a bright source the two contours are essentially identical.

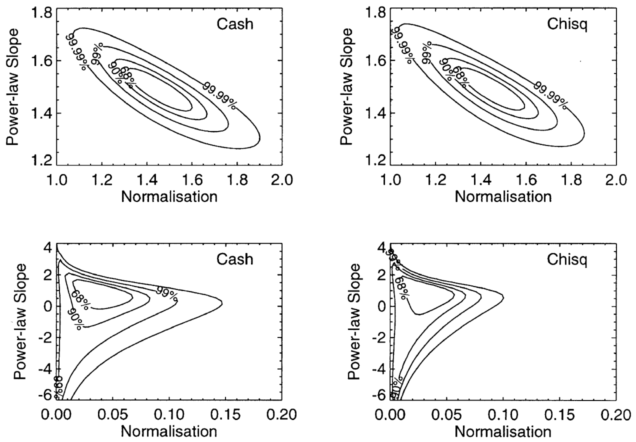

Figure 3. Confidence limits both for a bright source (upper panels) and a faint source near the Poisson limit (lower panels). The left-hand panels shows the confidence contours obtained using the Cash statistic; the right-hand panels show the same confidence contours using χ^2. In the case of the bright source there is no appreciable difference between the two methods, but for the faint source the Cash method gives a better constrained slope.

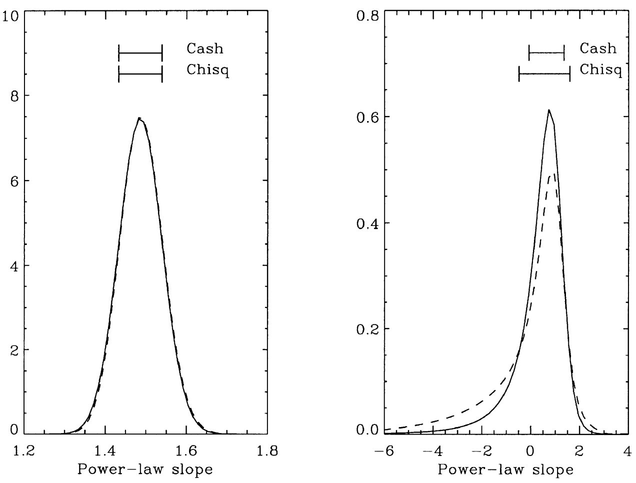

Figure 4. The marginalized ΔC statistic (which is related to the probability) as a function of spectral slope for a bright source (left-hand panel) and faint source (right-hand panel). The curves for both the χ^2 case (dashed) and the Cash statistic case (solid) are shown. Also shown are the corresponding marginalized errors for each case.

Owing to the lack of symmetry in the shape of the contours for sources near the Poisson limit, we have obtained marginalized errors (Loredo 1990, and references therein). These errors are obtained by integrating the ΔC values over the unwanted parameters, leaving a one-dimensional probability for the parameter of interest. This then gives us both the most probable value and the confidence intervals for the parameter of interest in a way that is statistically independent of any other parameters. The solid lines in Fig. 4 show the probability curves for the power-law slope for both a weak and a strong source. In the case of the weak source, the χ^2 probability curve and associated errors are larger than the corresponding Cash curves. For the bright source they are essentially identical. This is precisely the behaviour expected, as the Cash statistic is the same as χ^2 in the limit of large numbers, and shows the decrease in the size of the errors bars when the correct statistic is used.

5.3 Tests of the method

We have adopted a novel approach to the fitting of our data, and to convince ourselves of their reliability we have run stringent tests. In particular, we have investigated the improvement gained by using the correct statistic relative to using a simple hardness ratio. In the hardness-ratio method the error is normally derived assuming Gaussian errors of the form $\sqrt{(counts)}$, which in the extreme Poisson limit is no longer strictly true. In order to investigate this, we have generated a simulated data set where each of the sources has a known input spectrum but the normalization of the model has been scaled to give the same number of total counts as each of our real sources. The individual observed counts in each colour for each source have then been randomly obtained assuming Poisson statistics. In this way, we have a similar range of total observed counts and backgrounds to that of our real sample but with well-defined spectral characteristics. To compare this with the results for the AGN in the RIXOS sample, the power-law slopes were drawn from a Gaussian distribution of slopes with a mean of $\alpha = 1$ and a dispersion of $\sigma = 0.4$. The simulated data were then fitted in exactly the same way as the real data, and the power-law slopes and errors were determined from the marginalized errors. Fig. 5 shows the fitted slope minus the input slope for each source as a function of the source counts, and shows that the Cash method can recover the correct slope over a large flux range. Further, from our fitted slopes and errors we have estimated the average power-law slope and dispersion using the method outlined in Nandra & Pounds (1994) and Maccacaro et al. (1988). However, instead of assuming Gaussian statistics when dealing with the errors, we use the probability curves derived from the ΔC surfaces. The confidence limits of the mean power-law slope and intrinsic dispersion from the simulated data are shown in Fig. 6. The results are in excellent agreement with the input values, giving $\alpha = 1.02 \pm 0.05$ and $\sigma = 0.36 \pm 0.05$. We have also analysed the same data set using a hardness-ratio method, where we have used the ratio $S/(H1 + H2)$ to estimate the spectral slope together with an error based on Gaussian statistics. We have determined the average power-law slope and intrinsic dispersion of the sources from the hardness ratios, and the result is shown by the dashed contours. A comparison between the result obtain by using the Cash statistic and the hardness-ratio method shows that the hardness ratio result is marginally biased towards steeper (softer) slopes. It is likely that some bias may be caused by the failure of the hardness-ratio methods to take into account the Poissonian nature of the data, so this effect will depend on how many faint sources (i.e., with few counts) are contained within any given sample. Therefore it is possible that the use of a hardness ratio may have caused some bias in the results of previous surveys.

6 MODEL FITS TO THE RIXOS DATA

As we have limited resolution with three colours, our initial model is a simple power law. For each extragalactic source we have fixed the value of the Galactic N_H at the Stark et al. (1992) H I value and left the normalization and slope as free parameters. For the stars we have simply set the N_H at zero. Each source is fitted using the relevant response matrix for the source position and date of observation. The assumption of a power-law fit to all classes of objects is clearly incorrect for many of the sources (e.g., the stars and clusters), so these fits are only indicative of the overall slope

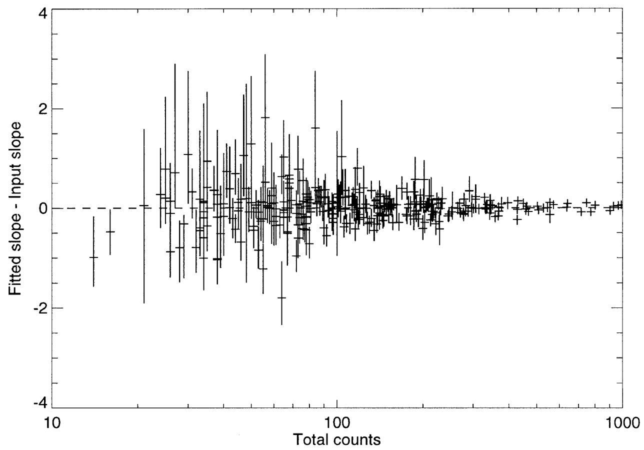

Figure 5. The fitted slope minus input slope for the simulated data. It is clear that the Cash method can recover the correct power-law slope over a large range of source counts.

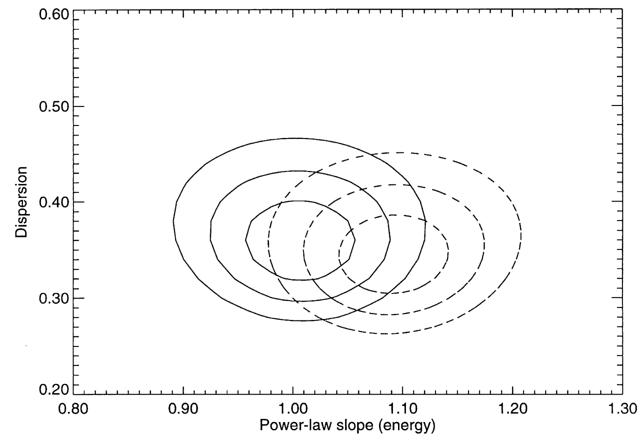

Figure 6. Estimated mean power-law slope and dispersion based on the simulated data for both the three-colour method (solid line) and the hardness-ratio method (dashed line). It is clear that the three-colour method gives the same answer as the input parameters to the simulation, whereas the hardness-ratio method has a bias towards steeper slopes.

of the X-ray spectrum. However, for the AGN it is likely to be fairly representative of the true flux distribution from many of the sources.

All of the fitted slopes are listed in Table 2. They have been determined in two different ways. Column 14 quotes the marginalized slope and error derived in a way which is independent of the value of the normalization (see Section 5.2 for details). Columns 15 and 16 of Table 2 list the normalization and slope derived from the minimum on the Cash surface for each source. As the marginalized slopes are independent of the other parameters, we have used this value in all subsequent plots rather than the value derived from the minimum of the Cash surface. The flux derived from the fits is given in column 17, where the error on the flux has been obtained by folding the flux calculation through the Cash contour. This flux may differ from the flux used to establish the sample, since the fitted slope may be significantly different from a slope of 1. Further, for uniformity all sources have been treated as point-like in the present analysis, and no attempt has been made to correct for extended sources, which was done in deriving the original fluxes. Fig. 7 shows the distribution of slopes for each class of objects. Essentially, the distribution of slopes

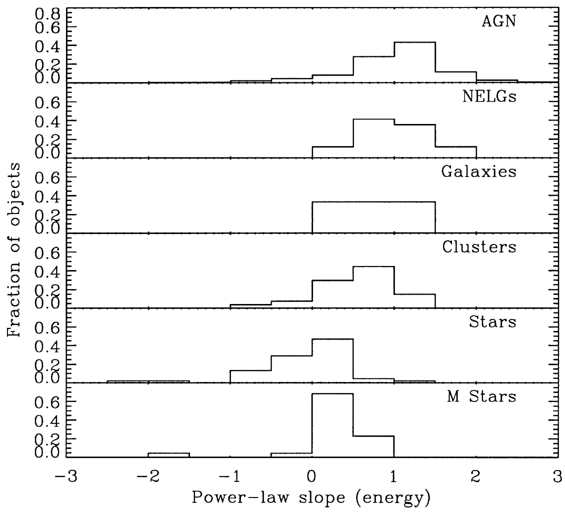

Figure 7. Histograms showing the distribution of the fitted power laws divided into different object classes.

again indicates differences between the AGN/NELGs and the clusters and stars. However, with the fitted data, we can investigate the intrinsic spectrum of the individual classes of sources in more detail.

6.1 The stars

The average power-law slope for the stars is $\alpha = 0.40$, implying that as a class they are hard sources. However, a power-law fit to the data is unlikely to be a good representation of the stellar X-ray emission. Although no simple way exists to determine the goodness of fit directly from the Cash statistic, it is possible to distinguish between good and bad fits to the data. To do this, we have calculated the expected number of counts based on the fitted model, subtracted the actual observed counts, and divided by the square root of the observed counts (an estimate of the error on the source counts). Fig. 8 shows this quantity for the best-fitting power-law model for each of the three colours for each star. It is clear from this plot that a power-law fit is not a good model of the stellar X-ray emission. It consistently overestimates the S1 and H2 bands, while consistently underestimating the H1 band. This distribution of the data relative to a power-law fit is, however, entirely consistent with the emission arising from warm (< 3 keV) gas. Such temperatures give rise to a large amount of line emission, particularly around the iron complex at 1 keV, and this line emission is the most likely explanation for the deviations seen in the three-colour data, particularly in the medium band.

With only three-colour data, it is not possible to fit the multitemperature models known to be required for X-ray spectra of stars (e.g. Schmitt et al. 1990). We have, however, fitted a single-temperature Raymond and Smith model (Raymond & Smith 1977) to our data. Fig. 9 shows the predicted minus observed counts with respect to the Raymond and Smith fits for the stars. It is clear that there is a marked improvement over the power-law fits, demonstrating that three-colour data are capable of distinguishing between thermal and non-thermal models.

6.2 The clusters

Fig. 10 shows the predicted minus observed distribution for each of the three bands for power-law fits to the cluster data. From this,

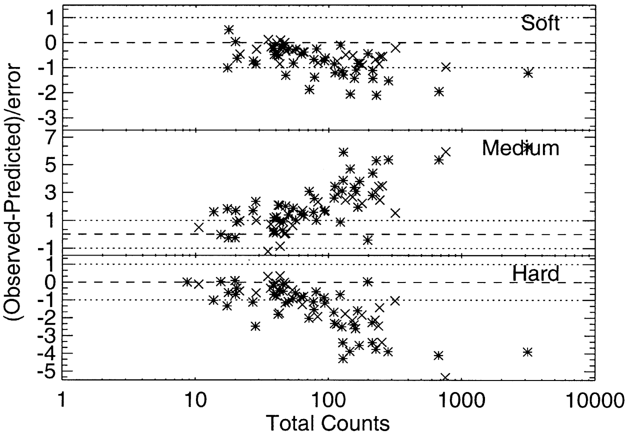

Figure 8. The predicted minus observed counts relative to a power-law model for the stars. The dotted lines denote 1σ around zero. The different symbols denote the two different types of stars in the RIXOS sample (* stars and × dMe stars).

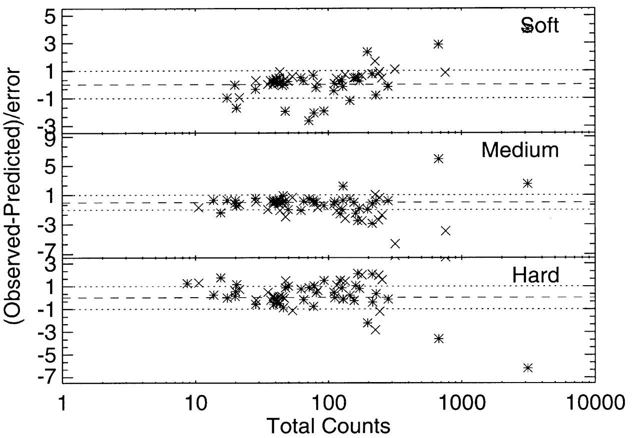

Figure 9. The predicted minus observed counts relative to a Raymond and Smith model for the stars. The dotted lines denote 1σ around zero. The use of a Raymond and Smith model has improved the goodness of fit for many of the stars.

it is apparent that a power-law fit is a reasonable representation of the data for most, though not all, clusters. At face value, this may seem surprising, since it is known that cluster emission arises from hot (2–10 keV) intergalactic gas, with some clusters showing evidence for a cooling flow (e.g. Sarazin 1986). However, because of the low energy of the *ROSAT* passband (0.1–2 keV), a hot plasma spectrum (>3 keV) is fairly well modelled by a power law with a slope $\alpha \sim 0.5$. This power-law slope is relatively insensitive to temperature and N_H. If we determine the average slope for the clusters, we find a mean of $\alpha = 0.5 \pm 0.05$, which is in agreement with that expected for a bremsstrahlung model with a temperature $kT > 3$ keV. There are, however, a number of clusters which, like the stars, show deviations from a simple power law, and it is likely that these objects have temperatures lower than 3 keV.

As the use of a single-temperature Raymond and Smith model reduced the residuals to the fit for the stars, we have attempted to fit a similar model to the three-colour data for the clusters. However, unlike the stars we find that in some cases a single-temperature model does not reduce the residuals. This was particularly true of 240-564, the brightest source in our sample,

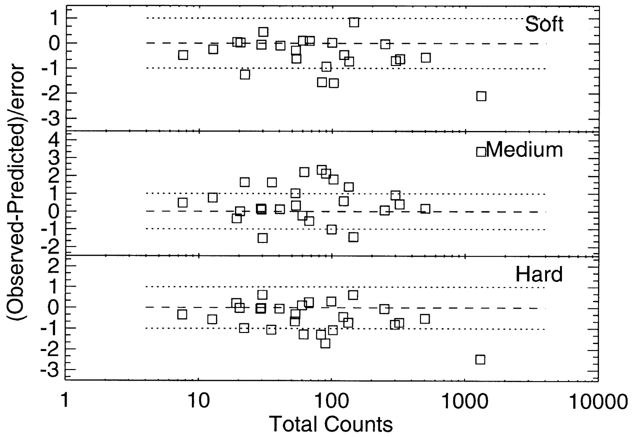

Figure 10. The predicted minus observed counts for the clusters. The dotted lines denote 1σ around zero.

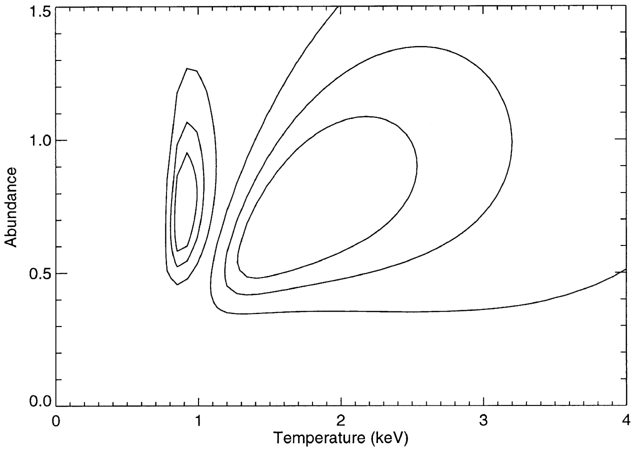

Figure 11. Colour plot of the Raymond and Smith fit to 240-564 in two regions, one in the innermost arcminute, the other from an annular region surrounding the central core. There is a clear cooling of the temperature between the inner regions and the outer regions.

where a single-temperature fit to the three-colour data gave a high (>10 keV) temperature. Based on the residuals to a power-law fit, 240-564 would be expected to have a relatively low temperature. For this object we have been able to extract a high-resolution spectrum, which we have fitted using XSPEC. Fig. 11 shows the fits both to the central region of the cluster and to an annular region surrounding the centre. As expected from the residuals, the temperature is low. There is also an apparent reduction in temperature towards the centre, implying that this cluster at least has a cooling flow. It is therefore clear that since three-colour data gave a *high* temperature, we cannot use the temperatures derived for the clusters with any degree of certainty. We have extended the method to four or five colours on a number of the clusters within the RIXOS sample, and this work shows that, with the extra channels, the method gives results that are consistent with higher resolution data. Such an extension to more colours is beyond the scope of this paper, however.

6.3 The narrow-emission-line objects

A subject of great interest is the X-ray emission from NELGs. Studies of the $\log N$–$\log S$ relation in fainter surveys such as the

Table 2. Table of X-ray data for the RIXOS sample.

FID	SRC	N_H $\times10^{20}$	Date	Exposure ksec	Radius arcmin	f_x(orig) $\times10^{-14}$	C1	C2	C3	B1	B2	B3	α_{1d}	Norm$_{2d}$ $\times10^{-5}$	α_{2d}	f_x(fit) $\times10^{-14}$	Object Type	Redshift
110	1	1.07	1991-Jul-22	23.69	0.90	6.54	492	68	67	73.08	7.29	4.26	$1.69^{+0.09}_{-0.06}$	2.84	1.71	6.57 ± 0.61	AGN	0.364
110	8	1.07	1991-Jul-22	23.69	0.90	3.07	142	31	34	75.15	7.50	4.38	$1.04^{+0.16}_{-0.15}$	1.58	1.06	3.45 ± 0.66	AGN	0.938
110	34	1.07	1991-Jul-22	23.69	0.90	3.07	86	24	37	74.90	7.47	4.37	$0.03^{+0.36}_{-0.47}$	1.22	0.04	3.00 ± 0.49	AGN	0.420
110	35	1.07	1991-Jul-22	23.69	0.90	3.05	216	20	31	74.69	7.45	4.35	$1.68^{+0.14}_{-0.14}$	1.14	1.70	2.61 ± 0.44	AGN	0.582
110	50	1.07	1991-Jul-22	23.69	0.90	3.91	154	26	38	81.09	8.09	4.73	$1.02^{+0.16}_{-0.15}$	1.24	1.02	2.73 ± 0.48	AGN	1.340
122	1	4.12	1991-Oct-18	30.33	0.90	4.40	97	38	53	59.72	12.14	5.37	$1.39^{+0.22}_{-0.28}$	1.71	1.41	3.81 ± 0.46	AGN	1.134
122	13	4.12	1991-Oct-18	30.33	0.48	8.85	25	55	128	19.03	3.87	1.71	$0.00^{+0.27}_{-0.28}$	3.76	0.00	9.18 ± 0.72	AGN	0.358
122	14	4.12	1991-May-29	30.33	0.78	7.61	125	87	80	45.15	9.18	4.06	$1.64^{+0.12}_{-0.12}$	3.15	1.65	7.23 ± 0.59	AGN	0.380
122	21	4.12	1991-May-29	30.33	0.90	8.70	65	70	112	60.98	12.40	5.49	$0.23^{+0.26}_{-0.28}$	4.02	0.23	9.50 ± 0.80	AGN	0.376
123	1	1.22	1991-May-29	19.89	0.90	17.71	629	133	140	54.17	8.38	4.54	$1.47^{+0.07}_{-0.04}$	7.29	1.49	16.52 ± 1.04	AGN	0.282
123	27	1.22	1991-May-29	19.89	0.90	4.42	133	44	43	57.46	8.89	4.82	$0.97^{+0.13}_{-0.13}$	1.97	0.98	4.54 ± 0.73	AGN	0.351
123	28	1.22	1991-May-29	19.89	0.78	3.90	114	35	32	38.79	6.00	3.25	$1.15^{+0.13}_{-0.14}$	1.55	1.17	3.26 ± 0.45	AGN	0.212
123	41	1.22	1991-May-29	19.89	0.90	3.57	98	33	37	52.33	8.09	4.39	$0.76^{+0.16}_{-0.18}$	1.56	0.78	3.71 ± 0.51	AGN	1.818
123	42	1.22	1991-May-29	19.89	0.90	3.29	115	25	35	52.02	8.05	4.36	$1.04^{+0.17}_{-0.15}$	1.36	1.06	2.98 ± 0.59	AGN	0.477
123	46	1.22	1991-Jun-04	19.89	0.90	3.65	63	32	36	56.06	8.67	4.70	$0.05^{+0.27}_{-0.39}$	1.38	0.06	3.37 ± 0.54	AGN	1.288
123	66	1.22	1991-Jun-04	19.89	0.90	5.81	131	35	44	51.46	7.96	4.32	$1.06^{+0.13}_{-0.13}$	2.36	1.07	5.05 ± 0.79	AGN	0.494
123	85	1.22	1991-Jun-04	19.89	0.90	9.71	482	51	67	52.04	8.05	4.36	$1.87^{+0.11}_{-0.05}$	3.68	1.91	8.73 ± 0.86	AGN	0.652
125	14	5.04	1991-Jun-15	22.51	0.90	3.83	44	29	50	30.43	8.84	8.27	$0.96^{+0.36}_{-0.55}$	1.84	0.97	4.14 ± 0.59	AGN	:1.840
125	17	5.04	1991-Jun-15	22.51	0.90	7.19	72	58	77	32.16	9.34	8.74	$1.48^{+0.17}_{-0.19}$	3.22	1.48	7.26 ± 0.69	AGN	:0.440
126	1	1.95	1991-Jun-15	10.80	0.90	9.04	55	23	61	33.89	6.03	4.17	$0.14^{+0.28}_{-0.40}$	4.12	0.15	9.95 ± 1.24	AGN	0.029
126	27	1.95	1991-Jun-15	10.80	0.60	12.86	50	40	62	14.91	2.65	1.84	$0.67^{+0.16}_{-0.14}$	5.26	0.68	12.12 ± 1.23	AGN	3.305
127	3	1.71	1991-Jun-15	20.21	0.90	7.56	267	51	51	55.48	10.03	6.34	$1.77^{+0.13}_{-0.07}$	2.49	1.82	5.84 ± 0.66	AGN	1.038
127	4	1.71	1991-Jun-15	20.21	0.90	5.26	161	42	44	51.09	9.24	5.84	$1.47^{+0.12}_{-0.12}$	2.51	1.49	5.62 ± 0.71	AGN	:0.975
127	17	1.71	1991-Jun-15	20.21	0.90	3.43	118	27	44	57.33	10.37	6.55	$1.13^{+0.16}_{-0.18}$	1.64	1.14	3.47 ± 0.49	AGN	:2.200
127	21	1.71	1991-Jun-15	20.21	0.90	7.70	144	45	75	55.99	10.13	6.40	$0.97^{+0.12}_{-0.12}$	3.07	0.98	7.01 ± 0.86	AGN	0.152
133	17	1.19	1990-Jun-20	6.17	0.90	3.40	18	4	11	14.37	1.53	1.35	$-0.25^{+0.78}_{-1.78}$	1.13	−0.39	3.18 ± 1.02	AGN	2.390
133	22	1.19	1990-Jun-20	6.17	0.90	5.94	42	14	19	14.30	1.53	1.34	$0.80^{+0.20}_{-0.20}$	2.71	0.83	6.64 ± 1.20	AGN	1.788
133	24	1.19	1990-Jun-20	6.17	0.90	4.15	20	4	14	14.99	1.60	1.41	$-0.35^{+0.83}_{-1.88}$	1.32	−0.49	6.64 ± 1.20	AGN	0.360
205	22	4.31	1991-Apr-10	9.62	0.90	10.98	59	35	46	15.16	2.97	2.47	$1.65^{+0.16}_{-0.17}$	4.62	1.66	10.61 ± 1.21	AGN	:0.440
205	23	4.31	1991-Apr-10	9.62	0.90	7.83	33	23	38	15.03	2.94	2.44	$1.14^{+0.27}_{-0.29}$	3.66	1.16	8.10 ± 1.14	AGN	0.618
205	34	4.31	1991-Apr-10	9.62	0.90	3.71	20	13	13	15.11	2.96	2.46	$1.20^{+0.50}_{-0.63}$	1.31	1.26	2.93 ± 0.75	AGN	0.754
206	6	3.65	1991-Apr-13	13.56	0.90	5.40	32	24	42	19.47	2.50	2.44	$0.67^{+0.30}_{-0.34}$	2.69	0.68	6.24 ± 0.82	AGN	0.690
206	9	3.65	1991-Apr-13	13.56	0.90	5.81	26	25	40	19.15	2.46	2.40	$0.48^{+0.33}_{-0.37}$	2.58	0.49	6.06 ± 0.82	AGN	:0.805
206	507	3.65	1991-Apr-13	13.56	0.90	6.00	28	19	21	19.68	2.52	2.47	$0.97^{+0.37}_{-0.38}$	1.49	1.01	3.39 ± 0.65	AGN	0.484
206	522	3.65	1991-Apr-13	13.56	0.90	9.00	38	23	23	18.62	2.39	2.33	$1.38^{+0.24}_{-0.26}$	1.76	1.40	3.86 ± 0.62	AGN	0.740
208	2	0.73	1991-Mar-08	15.22	0.90	11.72	400	62	86	36.72	3.51	2.55	$1.28^{+0.08}_{-0.06}$	5.07	1.30	11.25±0.94	AGN	0.387
208	18	0.73	1991-Mar-08	15.22	0.90	7.12	252	45	32	29.85	2.85	2.08	$1.47^{+0.13}_{-0.07}$	3.11	1.52	7.02±0.86	AGN	0.471
208	55	0.73	1991-Mar-08	15.22	0.90	5.14	98	26	36	36.38	3.48	2.53	$0.76^{+0.15}_{-0.13}$	2.12	0.78	5.01 ± 0.65	AGN	1.718
211	30	3.95	1991-Mar-08	14.30	0.90	6.61	36	31	39	22.69	5.84	3.10	$0.95^{+0.25}_{-0.34}$	2.79	0.97	6.31 ± 0.89	AGN	1.397
211	35	3.95	1991-Feb-09	14.30	0.60	4.24	22	17	25	11.37	2.93	1.55	$1.12^{+0.35}_{-0.38}$	1.71	1.14	3.81 ± 0.66	AGN	0.465
211	42	3.95	1991-Feb-09	14.30	0.90	7.32	67	39	48	24.63	6.34	3.36	$1.49^{+0.16}_{-0.19}$	3.24	1.50	7.27 ± 0.84	AGN	0.232
212	6	1.19	1991-Mar-17	6.88	0.90	4.84	41	10	16	19.68	2.06	1.45	$0.84^{+0.23}_{-0.29}$	2.01	0.87	4.93 ± 1.11	AGN	1.004

Table 2 – *continued*

FID	SRC	N_H $\times 10^{20}$	Date	Exposure ksec	Radius arcmin	f_x(orig) $\times 10^{-14}$	C1	C2	C3	B1	B2	B3	α_{1d}	Norm$_{2d}$ $\times 10^{-5}$	α_{2d}	f_x(fit) $\times 10^{-14}$	Object Type	Redshift
212	16	1.19	1991-Mar-17	6.88	0.90	3.52	38	12	11	18.48	1.93	1.36	$0.95^{+0.27}_{-0.26}$	1.63	1.00	3.85 ± 1.13	AGN	0.843
212	25	1.19	1991-Mar-17	6.88	0.90	5.41	73	14	17	18.29	1.91	1.34	$1.37^{+0.18}_{-0.17}$	2.38	1.40	5.16 ± 0.98	AGN	0.801
213	7	4.35	1991-Mar-17	6.27	0.90	6.60	11	19	16	10.05	4.98	1.69	$0.71^{+0.47}_{-0.57}$	2.50	0.74	5.75 ± 1.28	AGN	0.542
213	11	4.35	1990-Jul-19	6.27	0.90	3.15	7	9	13	10.29	5.10	1.73	$0.49^{+1.04}_{-1.77}$	1.17	0.88	3.60 ± 1.08	AGN	1.550
213	17	4.35	1990-Jul-19	6.27	0.90	8.66	15	20	11	8.76	4.34	1.47	$1.42^{+0.33}_{-0.44}$	2.95	1.46	6.48 ± 1.49	AGN	0.438
213	19	4.35	1990-Jul-19	6.27	0.90	7.88	22	23	19	9.98	4.94	1.68	$1.41^{+0.28}_{-0.32}$	3.43	1.45	7.58 ± 1.37	AGN	0.467
213	20	4.35	1990-Jul-19	6.27	0.90	7.60	15	20	19	9.60	4.75	1.61	$1.01^{+0.38}_{-0.46}$	3.37	1.04	7.58 ± 1.50	AGN	0.664
215	1	1.18	1991-Apr-12	8.43	0.90	3.43	64	12	22	26.40	3.19	2.32	$0.98^{+0.18}_{-0.22}$	1.91	1.01	4.40 ± 1.10	AGN	2.248
215	19	1.18	1991-Apr-12	8.43	0.90	8.86	160	27	38	26.49	3.20	2.33	$1.36^{+0.15}_{-0.07}$	3.75	1.41	8.30 ± 1.09	AGN	0.584
215	32	1.18	1991-Apr-12	8.43	0.90	3.57	56	13	11	24.71	2.99	2.17	$1.27^{+0.23}_{-0.26}$	1.40	1.32	2.86 ± 0.74	AGN	0.613
216	7	3.54	1991-Jun-26	14.70	0.90	4.09	37	24	33	24.72	4.67	3.69	$0.84^{+0.32}_{-0.36}$	1.95	0.86	4.49 ± 0.71	AGN	0.804
216	30	3.54	1991-Jun-26	14.70	0.84	5.11	39	27	36	22.95	4.33	3.42	$0.99^{+0.25}_{-0.31}$	2.37	1.00	5.36 ± 0.81	AGN	0.941
216	33	3.54	1991-Jun-26	14.70	0.90	3.46	32	22	22	23.19	4.38	3.46	$1.04^{+0.36}_{-0.39}$	1.76	1.06	3.96 ± 0.77	AGN	0.795
217	3	1.13	1991-Jun-26	21.74	0.90	3.71	183	39	39	76.22	8.75	4.85	$1.21^{+0.12}_{-0.13}$	1.59	1.22	3.41 ± 0.45	AGN	0.990
217	21	1.13	1991-May-09	21.74	0.84	3.31	170	28	40	65.78	7.55	4.19	$1.29^{+0.13}_{-0.13}$	1.85	1.31	4.02 ± 0.55	AGN	0.562
217	34	1.13	1991-May-09	21.74	0.90	4.62	245	42	51	77.46	8.89	4.93	$1.36^{+0.10}_{-0.10}$	2.00	1.37	4.43 ± 0.52	AGN	1.200
217	35	1.13	1991-May-09	21.74	0.90	3.60	154	29	48	78.32	8.99	4.99	$0.92^{+0.14}_{-0.15}$	1.67	0.94	3.96 ± 0.56	AGN	0.435
217	59	1.13	1991-May-09	21.74	0.90	5.24	200	42	61	67.93	7.80	4.32	$1.14^{+0.11}_{-0.10}$	2.97	1.14	6.34 ± 0.69	AGN	:0.590
218	1	3.01	1991-May-09	5.37	0.90	9.59	20	20	24	8.02	1.07	1.04	$0.85^{+0.25}_{-0.28}$	4.79	0.87	11.22 ± 1.84	AGN	0.545
218	9	3.01	1991-Jun-07	5.37	0.90	4.26	20	9	7	8.49	1.13	1.10	$1.50^{+0.39}_{-0.34}$	1.38	1.59	3.01 ± 0.85	AGN	:0.700
218	13	3.01	1991-Jun-07	5.37	0.42	3.93	6	4	8	2.08	0.28	0.27	$1.01^{+0.54}_{-0.68}$	1.43	1.08	3.37 ± 1.02	AGN	1.450
218	14	3.01	1991-Jun-07	5.37	0.42	10.44	15	8	22	2.03	0.27	0.26	$1.19^{+0.27}_{-0.26}$	3.85	1.21	8.38 ± 1.54	AGN	0.220
218	21	3.01	1991-Jun-07	5.37	0.90	4.27	6	7	14	7.77	1.04	1.01	$-0.32^{+0.70}_{-0.89}$	2.01	−0.37	5.46 ± 1.36	AGN	0.760
218	27	3.01	1991-Jun-07	5.37	0.90	13.61	29	18	30	8.00	1.07	1.04	$1.06^{+0.22}_{-0.21}$	5.51	1.07	12.23 ± 2.08	AGN	0.631
219	15	1.29	1992-Aug-29	20.17	0.90	3.06	248	34	44	89.69	17.56	7.90	$1.61^{+0.14}_{-0.11}$	1.53	1.63	3.47 ± 0.52	AGN	1.190
219	45	1.29	1992-Aug-29	20.17	0.48	8.49	67	49	74	23.91	4.68	2.11	$0.55^{+0.14}_{-0.13}$	4.30	0.55	9.91 ± 0.95	AGN	1.261
219	48	1.29	1992-Aug-29	20.17	0.90	3.12	118	37	27	83.72	16.39	7.38	$0.95^{+0.25}_{-0.24}$	1.27	0.98	2.94 ± 0.66	AGN	1.367
220	13	3.94	1992-Aug-29	6.36	0.90	3.04	10	4	14	8.49	1.64	1.39	$-0.89^{+1.94}_{-1.43}$	1.07	−1.51	3.86 ± 1.11	AGN	0.970
220	18	3.94	1992-Apr-23	6.36	0.90	4.42	11	8	11	7.94	1.53	1.30	$0.79^{+0.63}_{-0.83}$	1.85	0.83	4.37 ± 1.21	AGN	0.442
220	23	3.94	1992-Apr-23	6.36	0.90	7.02	8	7	17	6.68	1.29	1.10	$-0.14^{+0.81}_{-1.00}$	2.48	−0.22	6.63 ± 1.55	AGN	0.193
220	25	3.94	1992-Apr-23	6.36	0.90	5.83	28	13	12	7.51	1.45	1.23	$1.92^{+0.25}_{-0.28}$	2.51	1.97	5.98 ± 1.25	AGN	0.210
221	2	2.90	1992-Apr-23	9.93	0.90	3.90	34	14	22	19.15	4.73	2.65	$0.94^{+0.34}_{-0.41}$	1.74	0.98	4.00 ± 0.84	AGN	0.900
221	7	2.90	1992-Jul-02	9.93	0.90	24.75	105	86	116	18.37	4.54	2.54	$1.00^{+0.10}_{-0.10}$	11.88	1.00	26.47 ± 2.26	AGN	0.292
221	16	2.90	1992-Jul-02	9.93	0.90	6.61	70	23	25	18.22	4.50	2.52	$1.70^{+0.17}_{-0.17}$	2.35	1.73	5.40 ± 0.87	AGN	0.184
221	35	2.90	1992-Jul-02	9.93	0.90	52.26	168	144	229	16.77	4.14	2.32	$0.96^{+0.07}_{-0.07}$	24.37	0.96	55.13 ± 3.06	AGN	0.451
222	20	2.43	1992-Apr-01	12.89	0.90	3.00	60	22	17	29.83	3.76	2.84	$1.42^{+0.23}_{-0.22}$	1.43	1.45	3.12 ± 0.59	AGN	1.068
223	17	1.84	1990-Jun-21	36.12	0.90	11.76	625	161	199	130.60	9.99	5.85	$1.41^{+0.07}_{-0.04}$	5.54	1.42	12.15 ± 0.66	AGN	0.288
223	97	1.84	1991-May-08	36.12	0.54	4.93	86	56	76	49.07	3.75	2.20	$0.59^{+0.15}_{-0.17}$	2.07	0.60	4.62 ± 0.42	AGN	0.368
224	26	1.01	1991-Jun-02	19.37	0.42	8.99	31	53	81	14.57	1.55	0.94	$-0.01^{+0.15}_{-0.17}$	4.00	−0.01	9.74 ± 0.90	AGN	0.277
224	201	1.01	1991-Jun-02	19.37	0.42	4.39	85	30	31	12.51	1.33	0.81	$1.28^{+0.12}_{-0.13}$	1.82	1.29	3.96 ± 0.51	AGN	1.544
225	1	2.19	1991-Jun-02	18.12	0.84	3.17	49	22	28	16.23	3.12	2.76	$1.12^{+0.18}_{-0.20}$	1.39	1.13	2.94 ± 0.50	AGN	0.488
226	41	1.19	1991-May-30	38.13	0.90	9.58	569	174	184	154.53	37.28	9.79	$1.08^{+0.07}_{-0.04}$	4.38	1.09	9.59 ± 0.53	AGN	1.315

Table 2 – *continued*

FID	SRC	N_H $\times10^{20}$	Date	Exposure ksec	Radius arcmin	f_x(orig) $\times10^{-14}$	C1	C2	C3	B1	B2	B3	α_{1d}	Norm$_{2d}$ $\times10^{-5}$	α_{2d}	f_x(fit) $\times10^{-14}$	Object Type	Redshift
226	114	1.19	1991-May-30	38.13	0.84	3.74	198	66	73	118.40	28.56	7.50	$0.76^{+0.14}_{-0.14}$	2.08	0.77	4.81 ± 0.52	AGN	1.022
227	19	1.77	1991-Apr-10	25.32	0.90	3.67	164	45	48	54.25	8.45	4.81	$1.36^{+0.12}_{-0.12}$	1.73	1.37	3.84 ± 0.45	AGN	1.861
227	37	1.77	1991-Apr-10	25.32	0.90	9.72	243	92	106	51.64	8.05	4.58	$1.20^{+0.10}_{-0.05}$	4.90	1.23	10.80 ± 0.83	AGN	1.413
227	301	1.77	1991-Apr-10	25.32	0.90	3.77	649	49	47	55.56	8.66	4.93	$2.54^{+0.12}_{-0.06}$	1.59	2.58	4.31 ± 0.48	AGN	:0.114
227	513	1.77	1991-Apr-10	25.32	0.90	6.00	162	59	95	54.84	8.54	4.87	$0.91^{+0.10}_{-0.10}$	3.18	0.92	7.35 ± 0.64	AGN	0.959
228	1	3.66	1991-Apr-14	9.30	0.90	9.49	16	25	37	15.02	2.73	2.39	$0.27^{+0.37}_{-0.40}$	4.22	0.27	10.09 ± 1.43	AGN	1.726
229	11	0.79	1991-Apr-16	12.29	0.90	3.01	74	11	24	34.24	3.51	2.36	$0.85^{+0.20}_{-0.20}$	1.75	0.88	4.29 ± 0.82	AGN	1.419
229	40	0.79	1991-Apr-16	12.29	0.90	4.62	147	24	27	36.77	3.77	2.54	$1.30^{+0.13}_{-0.13}$	1.95	1.32	4.21 ± 0.65	AGN	1.252
229	301	0.79	1991-Apr-16	12.29	0.90	38.43	994	152	213	36.56	3.75	2.52	$1.36^{+0.05}_{-0.03}$	16.44	1.37	36.98 ± 1.95	AGN	0.175
231	301	0.73	1991-Nov-10	10.89	0.90	9.71	327	45	37	32.07	5.53	3.30	$1.62^{+0.12}_{-0.06}$	4.39	1.66	10.08 ± 1.23	AGN	0.783
231	302	0.73	1991-Nov-10	10.89	0.90	4.86	130	29	28	33.44	5.77	3.44	$1.13^{+0.13}_{-0.13}$	2.35	1.15	4.87 ± 0.74	AGN	1.572
232	16	0.84	1991-Mar-15	11.65	0.90	3.05	57	17	18	34.46	4.19	2.93	$0.64^{+0.25}_{-0.26}$	1.37	0.67	3.33 ± 0.67	AGN	0.227
232	301	0.84	1991-Feb-09	11.65	0.90	3.65	100	22	28	34.48	4.19	2.93	$0.97^{+0.15}_{-0.15}$	2.03	0.99	4.70 ± 1.04	AGN	0.385
234	1	4.05	1991-Feb-09	15.66	0.90	7.87	66	41	56	22.56	9.92	3.64	$1.48^{+0.15}_{-0.19}$	4.02	1.49	9.04 ± 0.99	AGN	1.666
234	33	4.05	1991-Feb-09	15.66	0.90	3.30	67	25	31	25.03	11.00	4.04	$1.94^{+0.22}_{-0.19}$	1.74	1.97	4.16 ± 0.66	AGN	1.019
236	5	2.55	1991-Feb-23	4.95	0.90	3.07	23	5	8	11.37	1.68	1.16	$1.37^{+0.43}_{-0.48}$	1.23	1.47	2.65 ± 0.89	AGN	0.473
236	21	2.55	1991-Mar-15	4.95	0.90	3.29	22	6	6	11.14	1.65	1.14	$1.48^{+0.41}_{-0.50}$	1.04	1.59	2.23 ± 0.81	AGN	1.130
236	22	2.55	1991-Mar-15	4.95	0.90	4.33	24	8	10	10.19	1.51	1.04	$1.34^{+0.33}_{-0.35}$	1.92	1.41	4.10 ± 1.09	AGN	0.048
237	15	2.95	1991-Mar-15	6.37	0.90	4.95	21	13	17	13.31	1.64	1.52	$0.82^{+0.37}_{-0.46}$	3.09	0.85	7.28 ± 1.53	AGN	0.158
238	11	4.08	1991-May-22	7.65	0.90	4.61	11	16	17	14.69	4.16	1.92	$0.29^{+0.54}_{-0.71}$	1.99	0.29	4.79 ± 1.05	AGN	0.325
240	15	1.22	1991-Aug-24	50.08	0.90	3.14	387	69	79	131.62	18.67	11.47	$1.43^{+0.10}_{-0.07}$	1.35	1.46	3.04 ± 0.30	AGN	1.263
240	82	1.22	1991-Aug-01	50.08	0.90	4.59	251	79	116	134.36	19.06	11.71	$0.70^{+0.11}_{-0.10}$	1.95	0.70	4.44 ± 0.37	AGN	0.518
245	4	8.81	1991-Aug-24	23.06	0.90	3.54	35	35	28	39.18	8.23	4.64	$1.86^{+0.40}_{-0.56}$	0.357	1.89	3.78 ± 0.58	AGN	:0.700
246	40	6.19	1991-Nov-14	22.47	0.90	5.87	44	37	69	39.15	8.29	6.25	$0.47^{+0.41}_{-0.51}$	2.67	0.47	6.18 ± 0.70	AGN	0.147
248	2	1.50	1992-May-12	19.55	0.90	7.84	145	58	82	51.51	8.17	4.77	$0.80^{+0.10}_{-0.11}$	3.67	0.81	8.49 ± 0.74	AGN	0.274
248	51	1.50	1992-May-12	19.55	0.90	13.70	456	109	123	52.97	8.41	4.91	$1.45^{+0.08}_{-0.04}$	6.45	1.47	14.58 ± 0.99	AGN	0.242
250	14	3.52	1991-Nov-14	19.37	0.72	5.24	41	26	51	19.63	2.49	2.55	$0.88^{+0.24}_{-0.28}$	2.63	0.90	6.02 ± 0.74	AGN	0.178
252	1	0.78	1991-Nov-14	11.89	0.90	5.25	76	20	27	36.53	4.43	2.70	$0.70^{+0.18}_{-0.19}$	2.61	0.72	6.24 ± 0.97	AGN	0.218
252	9	0.78	1991-Nov-14	11.89	0.90	3.61	136	22	25	46.43	5.63	3.44	$1.24^{+0.15}_{-0.14}$	1.81	1.27	3.82 ± 0.65	AGN	0.673
252	34	0.78	1992-May-03	11.89	0.90	3.09	95	17	22	46.80	5.67	3.46	$0.96^{+0.18}_{-0.20}$	1.40	0.98	3.33 ± 0.85	AGN	0.680
252	36	0.78	1992-May-08	11.89	0.90	6.05	150	27	38	46.77	5.67	3.46	$1.07^{+0.12}_{-0.12}$	2.63	1.08	5.47 ± 0.79	AGN	1.037
252	38	0.78	1992-May-08	11.89	0.90	12.43	297	70	62	45.36	5.50	3.36	$1.21^{+0.09}_{-0.06}$	5.81	1.23	12.73 ± 1.16	AGN	0.216
252	46	0.78	1992-May-08	11.89	0.90	5.22	170	27	22	44.92	5.44	3.32	$1.49^{+0.14}_{-0.14}$	1.92	1.52	4.26 ± 0.73	AGN	2.091
253	5	1.59	1992-May-08	14.81	0.90	3.03	75	25	18	37.99	4.10	3.73	$1.16^{+0.21}_{-0.19}$	1.25	1.19	2.61 ± 0.51	AGN	1.211
253	32	1.59	1992-May-08	14.81	0.90	4.25	104	24	26	35.20	3.80	3.46	$1.43^{+0.15}_{-0.16}$	2.11	1.44	4.64 ± 0.74	AGN	0.237
254	10	1.05	1991-Oct-30	9.08	0.90	11.38	318	34	55	37.83	3.34	1.99	$1.58^{+0.10}_{-0.07}$	5.17	1.60	11.78 ± 1.27	AGN	0.936
254	11	1.05	1991-Oct-30	9.08	0.90	8.76	169	25	38	38.30	3.38	2.01	$1.29^{+0.16}_{-0.07}$	3.58	1.34	7.86 ± 1.03	AGN	1.166
254	41	1.05	1991-Oct-30	9.08	0.90	4.02	70	13	12	29.95	2.64	1.57	$1.28^{+0.23}_{-0.20}$	1.54	1.33	3.19 ± 0.74	AGN	0.486
255	7	5.07	1991-Oct-30	7.36	0.90	3.32	13	9	11	9.16	2.73	2.03	$1.21^{+0.62}_{-1.05}$	1.64	1.29	3.71 ± 1.08	AGN	0.260
255	13	5.07	1991-Oct-30	7.36	0.90	4.08	15	15	8	10.86	3.24	2.40	$1.63^{+0.47}_{-0.56}$	1.30	1.70	2.94 ± 0.83	AGN	0.582
255	19	5.07	1992-Apr-17	7.36	0.90	4.06	24	11	10	10.66	3.18	2.36	$2.15^{+0.41}_{-0.39}$	1.24	2.24	3.09 ± 0.84	AGN	0.864
255	23	5.07	1992-Apr-17	7.36	0.90	4.36	11	12	11	10.46	3.12	2.31	$1.00^{+0.64}_{-0.80}$	1.55	1.05	3.48 ± 1.00	AGN	0.750

Table 2 – *continued*

FID	SRC	N_H $\times10^{20}$	Date	Exposure ksec	Radius arcmin	f_x(orig) $\times10^{-14}$	C1	C2	C3	B1	B2	B3	α_{1d}	Norm$_{2d}$ $\times10^{-5}$	α_{2d}	f_x(fit) $\times10^{-14}$	Object Type	Redshift
257	1	2.18	1992-Apr-17	11.47	0.90	16.55	150	73	81	18.57	3.81	2.18	$1.20^{+0.12}_{-0.06}$	7.29	1.23	16.05 ± 1.38	AGN	1.021
257	14	2.18	1991-Nov-26	11.47	0.90	4.75	34	23	24	17.35	3.56	2.04	$0.78^{+0.23}_{-0.27}$	2.22	0.80	5.24 ± 0.87	AGN	1.099
257	20	2.18	1991-Nov-26	11.47	0.90	3.44	35	16	16	18.57	3.81	2.18	$1.02^{+0.28}_{-0.31}$	1.34	1.06	3.04 ± 0.74	AGN	1.304
257	37	2.18	1991-Nov-26	11.47	0.90	3.31	32	15	13	18.54	3.80	2.18	$1.04^{+0.31}_{-0.36}$	1.17	1.09	2.62 ± 0.70	AGN	0.328
257	38	2.18	1991-Nov-26	11.47	0.90	4.29	39	14	22	18.18	3.73	2.14	$0.99^{+0.25}_{-0.29}$	2.03	1.02	4.65 ± 1.00	AGN	1.260
258	1	3.36	1991-Nov-26	13.03	0.90	15.13	25	51	97	24.62	3.78	2.95	$-0.18^{+0.25}_{-0.28}$	6.27	−0.18	15.75 ± 1.43	AGN	0.698
258	5	3.36	1991-Nov-23	13.03	0.90	4.09	49	22	17	24.51	3.77	2.93	$1.64^{+0.25}_{-0.26}$	1.53	1.68	3.47 ± 0.65	AGN	0.812
258	30	3.36	1991-Nov-23	13.03	0.90	3.09	39	8	31	25.37	3.90	3.04	$-1.07^{+1.89}_{-1.22}$	1.04	−1.74	2.55 ± 0.56	AGN	0.847
258	32	3.36	1991-Nov-23	13.03	0.90	3.26	36	18	24	25.98	3.99	3.11	$0.83^{+0.38}_{-0.48}$	1.56	0.85	3.60 ± 0.68	AGN	1.618
259	5	1.96	1992-May-12	10.55	0.90	5.64	60	22	30	26.53	3.68	2.56	$0.95^{+0.18}_{-0.22}$	2.49	0.97	5.75 ± 1.05	AGN	0.977
259	7	1.96	1992-May-12	10.55	0.84	3.42	36	18	21	25.43	3.53	2.45	$0.53^{+0.32}_{-0.38}$	1.72	0.55	4.09 ± 0.77	AGN	0.408
259	11	1.96	1992-May-12	10.55	0.60	3.34	30	12	18	13.03	1.81	1.26	$0.92^{+0.27}_{-0.28}$	1.47	0.96	3.45 ± 0.75	AGN	0.995
259	30	1.96	1992-Jul-12	10.55	0.90	4.84	34	20	32	25.99	3.61	2.50	$0.15^{+0.35}_{-0.42}$	2.51	0.16	6.10 ± 0.98	AGN	1.940
260	8	0.93	1992-Jul-12	9.96	0.90	3.71	66	17	18	24.42	2.91	2.51	$0.98^{+0.18}_{-0.19}$	1.59	1.00	3.66 ± 0.98	AGN	1.823
260	44	0.93	1992-Jul-16	9.96	0.90	3.84	44	11	26	23.44	2.80	2.40	$0.40^{+0.25}_{-0.30}$	2.33	0.42	5.61 ± 1.03	AGN	1.504
262	1	3.37	1991-Jun-23	12.12	0.90	3.45	35	14	19	13.69	3.27	2.87	$1.51^{+0.26}_{-0.28}$	1.39	1.56	2.90 ± 0.58	AGN	0.882
262	2	3.37	1991-Jun-23	12.12	0.90	4.79	34	20	28	13.74	3.28	2.88	$1.16^{+0.24}_{-0.26}$	2.07	1.18	4.26 ± 0.72	AGN	1.202
262	10	3.37	1991-Jun-23	12.12	0.90	22.43	125	101	122	14.26	3.41	2.99	$1.25^{+0.08}_{-0.09}$	10.40	1.25	21.80 ± 1.48	AGN	0.336
262	12	3.37	1991-Jun-23	12.12	0.90	5.61	38	26	28	14.02	3.35	2.94	$1.29^{+0.20}_{-0.24}$	2.40	1.31	4.93 ± 0.75	AGN	0.924
262	34	3.37	1991-Jun-23	12.12	0.78	9.32	61	40	46	10.77	2.57	2.26	$1.47^{+0.14}_{-0.14}$	4.42	1.48	9.39 ± 1.03	AGN	0.312
265	1	1.10	1991-Jun-23	12.02	0.90	7.88	100	30	47	34.94	4.15	3.31	$0.83^{+0.13}_{-0.13}$	3.51	0.84	8.30 ± 0.94	AGN	:2.340
265	17	1.10	1991-Dec-13	12.02	0.90	4.72	88	28	24	35.30	4.20	3.34	$1.00^{+0.15}_{-0.17}$	1.91	1.03	4.25 ± 0.93	AGN	0.448
266	32	2.05	1992-Jan-15	8.34	0.90	3.42	30	7	13	20.16	3.02	2.31	$0.78^{+0.55}_{-0.95}$	1.33	0.85	3.20 ± 0.95	AGN	2.460
266	527	2.05	1991-Mar-01	8.34	0.90	18.01	94	43	35	21.21	3.18	2.43	$1.34^{+0.13}_{-0.13}$	6.05	1.36	13.33 ± 1.60	AGN	0.135
268	11	2.08	1991-Mar-01	10.09	0.90	3.55	20	17	24	26.78	6.82	3.66	$-0.63^{+0.67}_{-0.87}$	1.42	−0.75	4.07 ± 0.91	AGN	1.196
268	24	2.08	1991-Mar-01	10.09	0.90	15.43	375	70	55	25.23	6.43	3.45	$2.09^{+0.10}_{-0.07}$	6.22	2.12	15.32 ± 1.43	AGN	0.251
270	3	3.57	1991-Mar-01	8.08	0.90	4.91	44	21	24	28.26	9.61	2.58	$1.14^{+0.38}_{-0.43}$	2.48	1.18	5.48 ± 1.06	AGN	0.220
270	4	3.57	1992-May-11	8.08	0.90	3.71	54	17	15	29.18	9.93	2.66	$1.86^{+0.33}_{-0.31}$	1.47	1.92	3.44 ± 0.84	:AGN	
270	14	3.57	1992-May-11	8.08	0.90	24.31	97	84	85	29.02	9.87	2.65	$1.28^{+0.12}_{-0.12}$	11.21	1.29	24.85 ± 2.00	AGN	0.121
270	18	3.57	1992-Apr-09	8.08	0.90	4.90	32	14	20	25.35	8.62	2.31	$0.44^{+0.76}_{-1.73}$	2.36	0.41	2.57 ± 0.90	AGN	0.258
271	2	2.07	1992-Apr-09	5.78	0.90	3.57	75	10	12	13.75	1.47	1.38	$2.03^{+0.21}_{-0.20}$	1.78	2.07	4.36 ± 0.99	AGN	0.446
271	7	2.07	1992-Apr-09	5.78	0.90	7.48	60	18	14	13.03	1.40	1.31	$1.65^{+0.19}_{-0.17}$	2.92	1.68	6.67 ± 1.25	AGN	1.039
272	8	4.67	1992-Apr-09	7.38	0.90	3.91	20	13	11	12.59	2.73	2.11	$1.54^{+0.42}_{-0.54}$	1.53	1.60	3.41 ± 0.86	AGN	:1.820
272	10	4.67	1992-Apr-09	7.38	0.90	12.93	40	35	36	11.88	2.57	1.99	$1.58^{+0.17}_{-0.21}$	5.44	1.59	12.35 ± 1.50	AGN	0.321
272	18	4.67	1992-Apr-09	7.38	0.90	9.24	26	17	35	11.68	2.53	1.96	$1.08^{+0.33}_{-0.40}$	5.30	1.10	11.89 ± 1.78	AGN	:0.590
272	23	4.67	1991-Nov-19	7.38	0.90	10.17	40	26	32	11.96	2.59	2.01	$1.65^{+0.19}_{-0.22}$	4.45	1.68	10.18 ± 1.37	AGN	0.095
272	28	4.67	1991-Nov-19	7.38	0.90	7.92	23	23	18	12.08	2.62	2.03	$1.46^{+0.28}_{-0.33}$	2.98	1.50	6.64 ± 1.16	AGN	0.440
273	4	2.81	1991-Nov-19	5.17	0.90	4.99	35	16	13	10.82	3.04	1.39	$1.52^{+0.24}_{-0.24}$	2.61	1.56	5.76 ± 1.21	AGN	1.046
273	6	2.81	1991-Nov-19	5.17	0.90	37.71	77	75	88	10.70	3.01	1.37	$0.96^{+0.11}_{-0.11}$	18.21	0.96	41.50 ± 3.73	AGN	0.270
273	18	2.81	1991-Nov-25	5.17	0.90	6.58	24	17	7	9.99	2.81	1.28	$1.49^{+0.28}_{-0.32}$	2.13	1.55	4.62 ± 1.17	AGN	0.361
273	22	2.81	1991-Nov-25	5.17	0.90	3.84	32	9	5	9.17	2.58	1.18	$2.15^{+0.34}_{-0.32}$	1.32	2.26	3.35 ± 1.12	AGN	1.080
274	8	2.16	1991-Nov-25	4.58	0.90	13.83	182	52	57	15.33	3.48	1.72	$1.66^{+0.11}_{-0.08}$	13.12	1.69	30.25 ± 2.97	AGN	0.156

Table 2 – *continued*

FID	SRC	N_H $\times10^{20}$	Date	Exposure ksec	Radius arcmin	f_x(orig) $\times10^{-14}$	C1	C2	C3	B1	B2	B3	α_{1d}	Norm$_{2d}$ $\times10^{-5}$	α_{2d}	f_x(fit) $\times10^{-14}$	Object Type	Redshift
277	1	1.74	1991-Nov-25	8.99	0.90	5.25	81	16	25	21.20	2.51	2.12	$1.44^{+0.16}_{-0.16}$	2.42	1.45	5.33 ± 0.88	AGN	0.595
278	9	1.94	1992-Jan-27	9.02	0.90	8.42	61	29	41	26.27	6.06	3.82	$0.80^{+0.19}_{-0.18}$	3.96	0.82	9.32 ± 1.20	AGN	0.949
278	10	1.94	1992-Jan-27	9.02	0.90	46.51	29	58	251	25.45	5.87	3.70	$-1.54^{+0.28}_{-0.30}$	15.18	−1.56	54.53 ± 3.78	AGN	0.090
279	1	4.28	1992-Jan-27	7.64	0.90	5.32	79	23	21	32.47	3.86	1.82	$2.20^{+0.20}_{-0.21}$	2.99	2.25	7.53 ± 1.19	AGN	1.146
279	6	4.28	1992-Jul-08	7.64	0.90	11.06	56	29	41	33.18	3.95	1.86	$1.19^{+0.25}_{-0.30}$	5.20	1.21	11.51 ± 1.47	AGN	0.180
279	27	4.28	1992-Aug-31	7.64	0.90	3.05	38	12	7	27.35	3.26	1.53	$1.95^{+0.49}_{-0.55}$	1.32	2.06	3.16 ± 0.94	AGN	0.620
281	11	5.76	1992-Aug-31	8.44	0.90	3.14	9	11	9	9.65	2.29	2.49	$1.15^{+0.66}_{-0.79}$	1.07	1.21	2.39 ± 0.74	AGN	2.930
281	21	5.76	1992-Aug-31	8.44	0.90	8.76	9	17	24	8.51	2.02	2.20	$0.67^{+0.49}_{-0.57}$	3.66	0.68	8.50 ± 1.48	AGN	0.349
283	6	10.46	1992-Aug-31	6.15	0.90	18.01	17	25	51	9.47	1.96	2.44	$1.07^{+0.52}_{-0.59}$	9.00	1.06	20.34 ± 2.50	AGN	1.219
283	11	10.46	1992-May-12	6.15	0.90	8.89	9	8	14	8.37	1.73	2.16	$1.05^{+1.11}_{-1.09}$	2.41	1.01	5.60 ± 1.44	AGN	0.272
283	14	10.46	1992-May-12	6.15	0.90	6.74	18	10	17	9.04	1.87	2.33	$2.50^{+0.76}_{-1.13}$	2.85	2.63	8.19 ± 1.18	AGN	0.284
283	21	10.46	1992-May-17	6.15	0.90	5.86	12	8	13	8.96	1.85	2.31	$1.48^{+1.10}_{-1.23}$	2.60	1.51	5.77 ± 1.34	AGN	0.724
286	2	2.33	1992-May-31	7.41	0.90	3.79	62	12	15	16.58	1.78	1.62	$1.82^{+0.22}_{-0.19}$	2.20	1.86	5.15 ± 1.05	AGN	1.498
290	21	1.46	1992-Jan-26	6.67	0.72	3.01	20	9	9	9.56	1.16	1.06	$0.84^{+0.34}_{-0.35}$	1.80	0.89	4.44 ± 1.25	AGN	2.575
292	8	3.48	1992-Apr-02	7.09	0.90	4.42	27	9	13	13.73	3.53	1.63	$1.47^{+0.39}_{-0.46}$	1.88	1.54	4.14 ± 1.06	AGN	0.594
292	11	3.48	1992-Apr-02	7.09	0.90	3.40	25	11	17	14.58	3.75	1.74	$1.05^{+0.46}_{-0.57}$	2.07	1.09	4.69 ± 1.09	AGN	0.655
292	19	3.48	1992-Apr-02	7.09	0.90	3.64	19	14	15	14.71	3.78	1.75	$0.73^{+0.50}_{-0.63}$	1.90	0.76	4.44 ± 1.05	AGN	:1.200
293	1	4.59	1992-Apr-02	7.10	0.90	6.36	24	13	19	19.39	2.27	1.76	$0.84^{+0.56}_{-0.67}$	2.51	0.86	5.77 ± 1.19	AGN	0.824
293	6	4.59	1992-Apr-02	7.10	0.90	14.70	45	38	47	20.65	2.42	1.88	$1.26^{+0.20}_{-0.23}$	6.85	1.27	15.14 ± 1.69	AGN	0.082
293	10	4.59	1991-Dec-03	7.10	0.90	16.36	40	36	47	19.39	2.27	1.76	$1.21^{+0.20}_{-0.26}$	7.50	1.22	16.55 ± 1.89	AGN	0.760
293	12	4.59	1991-Dec-03	7.10	0.90	4.46	23	9	14	20.37	2.39	1.85	$0.69^{+0.75}_{-1.05}$	1.75	0.69	4.11 ± 1.06	AGN	0.922
293	13	4.59	1991-Nov-01	7.10	0.90	6.60	24	14	29	19.89	2.33	1.81	$0.27^{+0.58}_{-0.72}$	3.30	0.25	7.99 ± 1.35	AGN	0.189
294	1	4.25	1991-Nov-01	9.23	0.60	5.27	15	16	22	4.25	0.94	0.92	$1.29^{+0.27}_{-0.33}$	2.62	1.32	5.77 ± 0.96	AGN	:0.710
299	106	1.56	1992-Oct-03	8.01	0.90	3.29	85	12	14	24.69	5.88	4.51	$1.89^{+0.28}_{-0.22}$	1.08	1.96	2.55 ± 0.76	AGN	0.735
302	14	1.23	1992-Oct-03	10.04	0.90	3.48	90	13	27	33.10	3.24	1.85	$1.15^{+0.16}_{-0.18}$	2.06	1.17	4.31 ± 0.73	AGN	0.811
302	18	1.23	1992-Oct-03	10.04	0.90	6.36	81	27	38	33.38	3.27	1.87	$0.74^{+0.15}_{-0.16}$	3.45	0.76	8.12 ± 1.07	AGN	0.950
303	105	3.55	1992-Oct-03	9.96	0.90	8.46	72	32	38	22.96	3.43	4.42	$1.63^{+0.17}_{-0.16}$	3.78	1.65	8.64 ± 1.11	AGN	0.680
303	106	3.55	1992-Nov-13	9.96	0.90	7.63	68	31	42	21.35	3.19	4.11	$1.55^{+0.16}_{-0.17}$	4.10	1.56	9.25 ± 1.15	AGN	0.329
303	107	3.55	1992-Nov-13	9.96	0.84	8.60	32	23	46	21.50	3.21	4.14	$0.40^{+0.36}_{-0.42}$	3.62	0.41	8.54 ± 1.16	AGN	2.100
303	110	3.55	1992-Nov-13	9.96	0.90	3.91	27	14	21	22.95	3.43	4.42	$0.59^{+0.51}_{-0.71}$	1.60	0.61	3.79 ± 0.85	AGN	1.392
304	29	3.56	1992-Oct-28	17.73	0.90	6.60	85	52	55	26.35	3.65	3.86	$1.45^{+0.14}_{-0.14}$	3.28	1.45	7.35 ± 0.74	AGN	1.480
304	30	3.56	1992-Oct-28	17.73	0.90	3.92	58	30	35	25.88	3.59	3.79	$1.38^{+0.21}_{-0.20}$	1.92	1.39	4.23 ± 0.57	AGN	0.680
304	48	3.56	1992-Oct-28	17.73	0.78	5.13	45	33	42	19.43	2.69	2.85	$1.12^{+0.20}_{-0.21}$	2.34	1.13	5.13 ± 0.66	AGN	1.163
305	11	2.25	1992-Oct-28	8.35	0.90	10.81	105	33	46	12.17	2.19	2.25	$1.45^{+0.12}_{-0.12}$	5.14	1.46	11.51 ± 1.32	AGN	0.252
305	18	2.25	1992-Oct-28	8.35	0.78	6.64	16	22	30	8.67	1.56	1.60	$0.28^{+0.26}_{-0.32}$	3.54	0.29	8.49 ± 1.29	AGN	0.386
305	30	2.25	1992-Oct-28	8.35	0.90	4.74	30	11	21	12.27	2.21	2.26	$0.94^{+0.27}_{-0.29}$	2.11	0.98	4.90 ± 1.08	:AGN	
305	34	2.25	1992-Oct-28	8.35	0.90	4.75	36	17	22	12.39	2.23	2.29	$1.06^{+0.22}_{-0.22}$	2.47	1.08	5.40 ± 1.12	AGN	0.854
122	16	4.12	1991-May-29	30.33	0.54	20.42	36	174	172	20.66	4.20	1.86	$0.71^{+0.12}_{-0.12}$	9.07	0.71	20.53 ± 1.15	NELG	0.006
124	36	1.64	1991-Jun-28	13.65	0.90	8.48	205	52	36	46.07	12.48	4.33	$1.70^{+0.15}_{-0.08}$	3.29	1.75	7.63 ± 0.99	NELG	0.343
205	25	4.31	1991-Apr-10	9.62	0.90	6.31	16	16	29	14.89	2.91	2.42	$0.20^{+0.55}_{-0.62}$	2.98	0.20	7.27 ± 1.26	NELG	0.196
217	5	1.13	1991-Jun-26	21.74	0.66	4.19	100	29	52	41.93	4.81	2.67	$0.74^{+0.13}_{-0.15}$	1.94	0.75	4.51 ± 0.54	NELG	0.137

Table 2 – *continued*

FID	SRC	N_H $\times10^{20}$	Date	Exposure ksec	Radius arcmin	f_x(orig) $\times10^{-14}$	C1	C2	C3	B1	B2	B3	α_{1d}	Norm$_{2d}$ $\times10^{-5}$	α_{2d}	f_x(fit) $\times10^{-14}$	Object Type	Redshift
217	560	1.13	1991-May-09	21.74	0.90	18.00	481	128	155	75.17	8.63	4.78	$1.18^{+0.07}_{-0.04}$	7.45	1.20	16.41 ± 0.94	NELG	0.095
219	26	1.29	1992-Aug-29	20.17	0.90	7.62	274	70	55	84.03	16.45	7.40	$1.45^{+0.10}_{-0.10}$	2.83	1.46	6.33 ± 0.70	NELG	0.124
226	74	1.19	1991-May-30	38.13	0.90	3.86	239	93	61	151.04	36.44	9.57	$0.91^{+0.12}_{-0.14}$	1.58	0.92	3.70 ± 0.45	NELG	0.303
231	307	0.73	1991-Nov-12	10.89	0.90	3.41	50	7	24	33.00	5.69	3.40	$0.15^{+0.96}_{-1.55}$	1.53	0.22	3.29 ± 0.17	:NELG	0.137
240	60	1.22	1991-Aug-24	50.08	0.60	4.08	283	85	97	66.38	9.42	5.78	$1.22^{+0.10}_{-0.05}$	2.06	1.25	4.54 ± 0.37	NELG	0.245
245	543	8.81	1991-Aug-24	23.06	0.90	63.46	73	192	241	40.68	8.55	4.82	$1.61^{+0.15}_{-0.15}$	3.75	1.61	37.38 ± 1.80	NELG	0.030
254	6	1.05	1991-Oct-30	9.08	0.66	5.63	39	13	32	20.28	1.79	1.06	$0.23^{+0.27}_{-0.28}$	2.59	0.25	6.23 ± 0.98	NELG	0.459
260	28	0.93	1992-Jul-16	9.96	0.90	5.75	85	20	32	24.29	2.90	2.49	$0.94^{+0.14}_{-0.15}$	2.85	0.96	6.79 ± 1.22	NELG	0.105
272	24	4.67	1991-Nov-19	7.38	0.90	3.19	12	7	8	11.95	2.59	2.00	$0.70^{+0.99}_{-1.41}$	0.87	0.73	2.04 ± 0.79	:NELG	0.17
273	23	2.81	1991-Nov-25	5.17	0.90	3.19	18	7	7	10.51	2.96	1.35	$1.24^{+0.56}_{-0.70}$	1.16	1.36	2.56 ± 0.97	NELG	0.433
278	15	1.94	1992-Jan-27	9.02	0.90	7.78	41	33	28	24.94	5.76	3.63	$0.63^{+0.21}_{-0.26}$	3.23	0.65	7.59 ± 1.16	NELG	0.080
294	6	4.25	1991-Nov-17	9.23	0.90	6.42	21	18	23	8.09	1.80	1.75	$1.27^{+0.27}_{-0.33}$	3.19	1.31	7.00 ± 1.19	:NELG	0.120
304	10	3.56	1992-Nov-13	17.73	0.66	11.03	24	47	107	13.61	1.89	1.99	$0.01^{+0.24}_{-0.26}$	4.94	0.01	12.02 ± 1.03	NELG	0.190
304	50	3.56	1992-Oct-28	17.73	0.90	3.71	30	21	27	24.17	3.35	3.54	$0.71^{+0.41}_{-0.43}$	1.78	0.72	4.14 ± 0.71	:NELG	0.088
224	3	1.01	1991-Jun-02	19.37	0.90	3.67	127	33	53	61.21	6.49	3.95	$0.71^{+0.13}_{-0.15}$	2.29	0.72	5.33 ± 0.64	:GAL	:0.360
231	503	0.73	1991-Nov-12	10.89	0.90	13.00	60	57	35	34.41	5.93	3.54	$0.77^{+0.16}_{-0.15}$	3.54	−0.11	8.91 ± 1.13	GAL	0.233
246	20	6.19	1991-Aug-01	22.47	0.90	8.03	47	85	71	40.74	8.63	6.50	$1.37^{+0.20}_{-0.22}$	3.96	1.37	8.89 ± 0.79	:GAL	0.043
277	8	1.74	1991-Nov-25	8.99	0.90	3.79	38	14	17	21.21	2.51	2.12	$0.79^{+0.27}_{-0.31}$	1.61	0.83	3.89 ± 0.82	:GAL	0.088
286	103	2.33	1992-May-31	7.41	0.66	3.98	11	9	11	8.71	0.93	0.85	$0.43^{+0.45}_{-0.67}$	1.63	0.46	4.01 ± 1.00	GAL	0.013
292	17	3.48	1992-Apr-02	7.09	0.90	4.46	14	15	14	14.65	3.76	1.74	$0.41^{+0.49}_{-0.71}$	1.79	0.43	4.27 ± 1.02	:GAL	0.135
122	552	4.12	1991-May-29	30.33	0.90	12.00	94	46	83	60.20	12.24	5.42	$0.89^{+0.25}_{-0.33}$	2.85	0.89	6.42 ± 0.64	:CLUS	:0.500
123	5	1.22	1991-May-29	19.89	0.72	3.60	68	39	27	35.52	5.49	2.98	$0.78^{+0.16}_{-0.19}$	1.62	0.80	3.85 ± 0.54	CLUS	0.061
123	560	1.22	1991-Jun-04	19.89	0.90	10.00	82	42	65	53.77	8.32	4.51	$0.19^{+0.18}_{-0.21}$	2.69	0.20	6.41 ± 0.72	CLUS	0.176
124	501	1.64	1991-Jun-14	13.65	0.90	94.00	181	142	241	45.41	12.30	4.27	$0.45^{+0.07}_{-0.08}$	18.46	0.45	42.32 ± 2.31	CLUS	0.167
127	514	1.71	1991-Dec-04	20.21	0.90	6.00	80	28	37	57.97	10.48	6.62	$0.58^{+0.28}_{-0.33}$	1.33	0.60	3.12 ± 0.51	:CLUS	:0.360
133	501	1.19	1990-Jun-20	6.17	0.90	11.00	20	6	4	14.45	1.54	1.36	$0.78^{+0.64}_{-0.75}$	0.60	0.93	1.48 ± 0.74	:CLUS	0.210
211	526	3.95	1991-Feb-09	14.30	0.30	11.00	3	4	4	2.49	0.64	0.34	$0.96^{+0.84}_{-1.21}$	0.99	1.05	2.34 ± 0.96	CLUS	0.268
213	522	4.35	1991-Apr-12	6.27	0.90	11.00	13	11	12	9.41	4.66	1.58	$0.92^{+0.61}_{-1.16}$	1.93	1.08	4.47 ± 1.28	CLUS	0.160
215	11	1.18	1991-Apr-12	8.43	0.90	4.04	64	14	22	26.94	3.26	2.37	$0.96^{+0.21}_{-0.19}$	2.06	0.99	4.81 ± 1.15	:CLUS	0.230
219	22	1.29	1992-Aug-29	20.17	0.90	3.19	148	33	40	94.65	18.53	8.34	$0.94^{+0.22}_{-0.19}$	1.35	0.97	3.13 ± 0.62	:CLUS	
221	511	2.90	1992-Jul-02	9.93	0.90	15.00	23	16	26	17.66	4.36	2.45	$0.26^{+0.50}_{-0.61}$	2.15	0.27	5.19 ± 0.97	:CLUS	0.218
222	504	2.43	1992-Apr-01	12.89	0.90	8.00	32	30	37	26.97	3.40	2.57	$0.27^{+0.31}_{-0.30}$	2.84	0.28	6.77 ± 0.94	:CLUS	
223	572	1.84	1991-Jun-02	36.12	0.90	4.00	126	43	35	133.94	10.25	6.00	$0.32^{+0.31}_{-0.33}$	0.86	0.33	1.96 ± 0.30	CLUS	0.244
226	552	1.19	1991-Apr-10	38.13	0.90	5.00	185	80	65	150.48	36.30	9.54	$0.36^{+0.18}_{-0.25}$	1.31	0.37	3.06 ± 0.37	CLUS	0.403
228	18	3.66	1991-Apr-14	9.30	0.90	34.57	124	102	117	15.44	2.80	2.46	$1.44^{+0.09}_{-0.10}$	14.52	1.44	32.65 ± 2.20	CLUS	0.335
231	526	0.73	1991-Mar-15	10.89	0.90	23.00	39	40	45	31.81	5.48	3.28	$-0.25^{+0.21}_{-0.26}$	4.09	−0.25	10.45 ± 1.37	CLUS	0.047
231	534	0.73	1991-Mar-15	10.89	0.90	8.00	43	13	17	34.37	5.93	3.54	$0.12^{+0.54}_{-0.74}$	1.06	0.15	2.65 ± 0.70	CLUS	0.296
234	505	4.05	1991-Feb-23	15.66	0.90	7.00	23	17	28	25.70	11.30	4.15	$-0.91^{+1.91}_{-1.23}$	1.00	−1.00	4.16 ± 0.66	CLUS	0.167
240	564	1.22	1991-Aug-01	50.08	0.90	53.84	428	406	636	129.25	18.34	11.26	$0.20^{+0.05}_{-0.05}$	14.30	0.20	33.61 ± 1.12	CLUS	0.081
246	508	6.19	1992-May-12	22.47	0.90	6.86	44	30	34	39.74	8.42	6.34	$1.26^{+0.43}_{-0.56}$	1.42	1.27	3.18 ± 0.51	CLUS	0.251

Table 2 – *continued*

FID	SRC	N_H $\times 10^{20}$	Date	Exposure ksec	Radius arcmin	f_x(orig) $\times 10^{-14}$	C1	C2	C3	B1	B2	B3	α_{1d}	Norm$_{2d}$ $\times 10^{-5}$	α_{2d}	f_x(fit) $\times 10^{-14}$	Object Type	Redshift
254	524	1.05	1991-Oct-30	9.08	0.90	42.00	27	3	4	12.97	1.14	0.68	$1.33^{+0.45}_{-0.43}$	0.49	1.49	0.96 ± 0.45	CLUS	0.010
258	101	3.36	1991-Nov-23	13.03	0.90	3.87	20	17	8	24.81	3.81	2.97	$0.82^{+0.52}_{-0.62}$	0.70	0.87	1.61 ± 0.52	CLUS	0.160
260	106	0.93	1992-Jul-16	9.96	0.90	4.04	44	18	18	22.09	2.64	2.27	$0.63^{+0.21}_{-0.25}$	2.11	0.65	5.10 ± 0.94	CLUS	0.250
265	505	1.10	1991-Dec-13	12.02	0.90	33.54	128	83	132	35.96	4.28	3.41	$0.36^{+0.09}_{-0.09}$	9.81	0.37	22.75 ± 1.67	CLUS	0.245
283	4	10.46	1992-Aug-31	6.15	0.90	3.34	7	5	11	9.37	1.93	2.41	$0.27^{+1.44}_{-1.75}$	1.26	−0.12	3.43 ± 1.34	:CLUS	0.164
283	8	10.46	1992-May-12	6.15	0.90	4.98	10	13	13	9.58	1.98	2.47	$1.98^{+0.72}_{-0.81}$	2.47	2.05	6.08 ± 1.42	:CLUS	0.320
285	514	3.43	1991-Dec-02	8.19	0.90	14.97	26	19	32	11.92	2.58	2.58	$0.83^{+0.27}_{-0.33}$	3.38	0.85	7.86 ± 1.23	CLUS	0.255
285	518	3.43	1992-May-31	8.19	0.90	18.31	23	7	17	11.77	2.55	2.54	$1.14^{+0.46}_{-0.64}$	1.60	1.20	3.62 ± 0.93	:CLUS	0.180
293	15	4.59	1991-Nov-01	7.10	0.90	6.19	13	21	18	18.29	2.14	1.66	$0.70^{+0.40}_{-0.48}$	3.76	0.71	8.79 ± 1.64	CLUS	0.082
294	519	4.25	1991-Nov-17	9.23	0.90	24.85	17	46	54	10.12	2.25	2.19	$0.61^{+0.24}_{-0.24}$	7.33	0.61	16.91 ± 1.79	CLUS	0.124
122	31	4.12	1991-May-29	30.33	0.90	7.84	112	114	81	61.03	12.41	5.49	$-0.17^{+0.11}_{-0.09}$	2.87	−0.17	7.15 ± 0.63	STAR	
125	5	5.04	1991-Jun-14	22.51	0.90	4.53	86	61	32	32.25	9.37	8.77	$0.25^{+0.13}_{-0.12}$	1.48	0.26	3.51 ± 0.50	:STAR	
127	539	1.71	1990-Jun-20	20.21	0.90	14.00	180	36	54	56.32	10.19	6.44	$0.59^{+0.10}_{-0.10}$	2.04	0.60	4.76 ± 0.58	:STAR	
211	34	3.95	1991-Feb-09	14.30	0.84	7.47	98	54	36	19.87	5.11	2.71	$0.38^{+0.11}_{-0.10}$	2.86	0.39	6.70 ± 0.84	:STAR	
213	1	4.35	1991-Mar-17	6.27	0.90	16.37	61	49	33	10.01	4.95	1.68	$0.18^{+0.12}_{-0.11}$	5.89	0.19	14.08 ± 1.85	:STAR	
216	28	3.54	1991-Jun-26	14.70	0.90	3.54	30	25	27	25.87	4.88	3.86	$-0.53^{+0.27}_{-0.35}$	1.31	−0.52	3.54 ± 0.66	:STAR	
219	1	1.29	1991-Jun-07	20.17	0.90	5.26	123	63	33	83.84	16.42	7.39	$0.21^{+0.14}_{-0.17}$	1.86	0.22	4.46 ± 0.70	:STAR	
222	9	2.43	1992-Apr-01	12.89	0.90	10.89	60	73	48	29.32	3.70	2.80	$-0.23^{+0.12}_{-0.12}$	4.05	−0.23	10.25 ± 1.10	STAR	
226	130	1.19	1991-May-30	38.13	0.90	4.23	289	140	52	153.17	36.95	9.71	$0.48^{+0.09}_{-0.09}$	1.51	0.48	3.50 ± 0.39	:STAR	
228	11	3.66	1991-Apr-14	9.30	0.90	3.62	35	10	14	15.24	2.77	2.43	$0.32^{+0.25}_{-0.24}$	1.36	0.36	3.37 ± 0.84	:STAR	
228	15	3.66	1991-Apr-14	9.30	0.90	16.75	120	60	54	15.32	2.78	2.44	$0.35^{+0.09}_{-0.09}$	6.28	0.36	14.68 ± 1.52	:STAR	
229	302	0.79	1991-Nov-10	12.29	0.90	5.15	65	26	27	34.96	3.58	2.41	$0.12^{+0.18}_{-0.17}$	1.99	0.13	4.82 ± 0.78	STAR	
232	302	0.84	1991-Feb-09	11.65	0.90	4.00	55	15	15	32.58	3.96	2.77	$0.32^{+0.22}_{-0.27}$	1.26	0.35	3.10 ± 0.72	:STAR	
238	16	4.08	1991-May-22	7.65	0.90	4.15	26	16	16	13.52	3.83	1.76	$-0.05^{+0.23}_{-0.30}$	2.10	−0.02	5.30 ± 1.19	:STAR	
238	21	4.08	1991-May-22	7.65	0.90	6.58	27	16	15	12.36	3.50	1.61	$0.05^{+0.25}_{-0.24}$	2.10	0.08	5.24 ± 1.17	STAR	
245	6	8.81	1991-Aug-24	23.61	0.90	8.78	53	88	60	43.53	9.16	5.16	$-0.46^{+0.14}_{-0.15}$	0.56	−0.46	6.41 ± 0.67	:STAR	
246	10	6.19	1991-Aug-01	22.47	0.90	3.29	48	29	30	38.54	8.16	6.15	$-0.31^{+0.26}_{-0.32}$	0.97	−0.30	2.50 ± 0.47	:STAR	
246	35	6.19	1991-Nov-14	22.47	0.90	9.02	83	66	59	38.03	8.05	6.07	$-0.07^{+0.11}_{-0.13}$	2.97	−0.06	7.30 ± 0.81	:STAR	
250	13	3.52	1992-May-12	19.37	0.72	5.53	36	31	50	19.33	2.45	2.51	$-0.42^{+0.19}_{-0.19}$	2.12	−0.42	5.60 ± 0.71	:STAR	
250	35	3.52	1991-Nov-14	19.37	0.90	4.66	44	36	40	33.42	4.23	4.34	$-0.46^{+0.20}_{-0.22}$	1.58	−0.46	4.20 ± 0.59	:STAR	
255	20	5.07	1992-Apr-17	7.36	0.90	3.07	10	4	17	10.63	3.17	2.35	$-3.64^{+1.75}_{-0.80}$	0.45	−3.67	3.09 ± 0.84	:STAR	
255	32	5.07	1992-Apr-17	7.36	0.90	3.01	10	3	11	10.61	3.17	2.35	$-1.96^{+1.29}_{-2.13}$	0.11	−6.18	2.32 ± 0.92	:STAR	
255	33	5.07	1992-Apr-17	7.36	0.90	3.46	11	10	15	10.27	3.07	2.27	$-0.85^{+0.60}_{-0.80}$	1.44	−0.87	4.36 ± 1.20	:STAR	
261	1	3.31	1992-Jul-16	12.85	0.90	9.16	109	60	32	23.39	3.60	2.99	$0.40^{+0.10}_{-0.09}$	3.31	0.41	7.75 ± 0.94	:STAR	
261	33	3.31	1992-Jul-16	12.85	0.90	6.53	31	38	34	24.63	3.80	3.14	$-0.50^{+0.20}_{-0.22}$	2.35	−0.49	6.30 ± 0.92	:STAR	
266	12	2.05	1992-Jan-15	8.34	0.90	3.05	124	16	11	22.43	3.36	2.57	$1.26^{+0.17}_{-0.17}$	1.31	1.30	2.66 ± 0.64	STAR	
268	7	2.08	1991-Mar-01	10.09	0.90	4.43	44	16	21	25.71	6.55	3.51	$0.02^{+0.26}_{-0.28}$	1.39	0.05	3.44 ± 0.76	:STAR	
270	13	3.57	1992-May-11	8.08	0.90	4.01	62	26	15	28.49	9.69	2.60	$0.48^{+0.19}_{-0.20}$	1.60	0.51	3.90 ± 0.89	:STAR	
271	27	2.07	1992-Apr-09	5.78	0.90	3.97	22	16	6	13.02	1.39	1.30	$0.12^{+0.29}_{-0.27}$	1.58	0.17	3.96 ± 1.05	:STAR	
272	9	4.67	1992-Apr-09	7.38	0.90	17.16	42	41	44	12.30	2.66	2.06	$-0.22^{+0.13}_{-0.14}$	5.25	−0.21	13.26 ± 1.64	STAR	
272	29	4.67	1991-Nov-19	7.38	0.66	3.02	8	11	7	6.28	1.36	1.05	$-0.31^{+0.38}_{-0.50}$	1.18	−0.27	3.15 ± 0.95	STAR	

Table 2 – *continued*

FID	SRC	N_H $\times 10^{20}$	Date	Exposure ksec	Radius arcmin	f_x(orig) $\times 10^{-14}$	C1	C2	C3	B1	B2	B3	α_{1d}	Norm$_{2d}$ $\times 10^{-5}$	α_{2d}	f_x(fit) $\times 10^{-14}$	Object Type	Redshift
273	14	2.81	1991-Jul-11	5.17	0.90	4.82	20	6	9	10.78	3.04	1.38	$0.07^{+0.37}_{-0.50}$	1.12	0.14	2.89 ± 0.94	STAR	
277	20	1.74	1992-Jul-18	8.99	0.90	5.90	44	21	25	20.51	2.42	2.05	$0.01^{+0.19}_{-0.18}$	2.42	0.03	5.99 ± 1.01	STAR	
278	26	1.94	1992-Jan-27	9.02	0.90	3.14	19	16	13	23.98	5.54	3.49	$-0.78^{+0.55}_{-0.85}$	0.89	−0.80	2.63 ± 0.83	:STAR	
279	12	4.28	1992-Jul-08	7.64	0.90	3.37	53	15	15	34.19	4.07	1.91	$0.16^{+0.25}_{-0.29}$	1.56	0.20	3.85 ± 0.89	:STAR	
281	1	5.76	1992-Aug-31	8.44	0.84	319.91	1404	729	1009	9.05	2.15	2.33	$0.19^{+0.03}_{-0.01}$	112.65	0.20	264.53 ± 6.67	STAR	
283	5	10.46	1992-Aug-31	6.15	0.90	3.70	9	10	8	9.32	1.92	2.40	$-0.54^{+0.50}_{-0.69}$	1.00	−0.51	2.79 ± 0.98	:STAR	
285	4	3.43	1992-May-17	8.19	0.90	8.44	41	23	35	12.67	2.74	2.74	$-0.09^{+0.14}_{-0.17}$	3.25	−0.08	8.09 ± 1.21	STAR	
286	9	2.33	1992-May-31	7.41	0.90	28.56	80	84	71	17.06	1.83	1.67	$-0.08^{+0.09}_{-0.09}$	10.96	−0.08	26.98 ± 2.40	:STAR	
288	15	1.43	1992-Jan-26	6.77	0.90	3.77	47	14	10	18.07	1.64	1.45	$0.53^{+0.20}_{-0.20}$	1.58	0.57	3.91 ± 0.89	STAR	
293	8	4.59	1991-Dec-03	7.10	0.90	4.55	40	18	9	20.85	2.44	1.89	$0.31^{+0.24}_{-0.22}$	1.45	0.35	3.59 ± 0.87	:STAR	
304	7	3.56	1992-Nov-13	17.73	0.66	3.05	47	24	19	13.52	1.88	1.98	$0.648^{+0.15}_{-0.15}$	1.13	0.63	2.71 ± 0.47	:STAR	
304	23	3.56	1992-Nov-13	17.73	0.90	3.50	36	11	34	15.85	2.20	2.32	$-0.22^{+0.24}_{-0.22}$	1.74	0.81	4.45 ± 0.75	:STAR	
305	33	2.25	1992-Nov-13	8.35	0.90	3.28	17	14	12	11.72	2.11	2.16	$-0.25^{+0.34}_{-0.36}$	1.52	−0.22	3.97 ± 1.01	:STAR	
122	10	4.12	1991-Oct-18	30.33	0.84	7.01	159	77	83	58.79	11.95	5.29	$0.12^{+0.09}_{-0.09}$	2.35	0.12	5.61 ± 0.53	DME	
126	12	1.95	1991-Jun-15	10.80	0.90	3.47	50	9	20	33.81	6.01	4.16	$0.05^{+0.38}_{-0.51}$	1.28	0.09	3.23 ± 0.84	:DME	
206	517	3.65	1991-Apr-13	13.56	0.90	5.00	33	10	18	18.04	2.31	2.26	$0.02^{+0.27}_{-0.30}$	1.00	0.05	2.49 ± 0.56	DME	
208	33	0.73	1991-Mar-08	15.22	0.90	4.95	138	40	34	39.60	3.79	2.75	$0.56^{+0.10}_{-0.11}$	2.22	0.57	5.18 ± 0.67	:DME	
212	1	1.19	1991-Mar-17	6.88	0.90	4.26	35	19	12	19.74	2.06	1.45	$0.13^{+0.24}_{-0.23}$	1.93	0.16	4.76 ± 1.03	DME	
216	21	3.54	1991-Jun-26	14.70	0.90	7.48	125	46	38	22.67	4.28	3.38	$0.55^{+0.10}_{-0.10}$	3.37	0.56	7.87 ± 0.96	DME	
220	1	3.94	1992-Aug-29	6.36	0.90	3.52	18	10	11	7.72	1.49	1.27	$0.01^{+0.27}_{-0.30}$	1.54	0.05	3.91 ± 1.00	DME	
220	11	3.94	1992-Aug-29	6.36	0.90	3.89	12	9	12	8.53	1.64	1.40	$-0.50^{+0.42}_{-0.55}$	1.33	−0.47	3.66 ± 1.00	DME	
220	14	3.94	1992-Apr-23	6.36	0.90	4.33	35	6	14	8.67	1.67	1.42	$0.45^{+0.21}_{-0.21}$	1.49	0.48	3.72 ± 0.89	DME	
221	9	2.90	1992-Jul-02	9.93	0.90	9.00	84	42	33	18.17	4.49	2.52	$0.34^{+0.12}_{-0.11}$	3.37	0.35	7.96 ± 1.07	DME	
223	73	1.84	1990-Jun-21	36.12	0.90	4.71	246	80	61	132.45	10.13	5.93	$0.32^{+0.09}_{-0.10}$	1.68	0.33	3.83 ± 0.39	DME	
228	14	3.66	1991-Apr-14	9.30	0.90	3.54	49	9	11	15.97	2.90	2.54	$0.76^{+0.22}_{-0.23}$	0.87	0.81	2.34 ± 0.61	DME	
258	20	3.36	1991-Nov-23	13.03	0.90	3.21	47	12	19	24.71	3.80	2.96	$0.20^{+0.25}_{-0.23}$	1.04	0.23	2.55 ± 0.56	DME	
259	1	1.96	1992-May-12	10.55	0.90	17.83	123	68	65	25.08	3.48	2.42	$0.22^{+0.09}_{-0.09}$	7.89	0.22	18.66 ± 1.79	:DME	
265	12	1.10	1991-Dec-13	12.02	0.90	3.18	62	15	17	33.27	3.96	3.15	$0.40^{+0.22}_{-0.21}$	1.30	0.44	3.17 ± 0.70	DME	
265	20	1.10	1991-Dec-13	12.02	0.90	4.32	77	30	19	35.42	4.21	3.35	$0.39^{+0.17}_{-0.15}$	1.59	0.41	3.80 ± 0.68	DME	
266	1	2.05	1991-Dec-13	8.34	0.90	23.91	474	191	120	21.22	3.18	2.43	$0.61^{+0.06}_{-0.03}$	20.25	0.62	46.00 ± 2.85	DME	
266	35	2.05	1992-Jan-15	8.34	0.90	3.48	21	4	16	18.44	2.76	2.11	$-1.67^{+1.67}_{-1.89}$	0.80	−3.00	5.02 ± 0.03	:DME	
268	3	2.08	1991-Mar-01	10.09	0.90	3.17	40	16	16	25.35	6.46	3.46	$0.08^{+0.29}_{-0.33}$	1.13	0.12	2.81 ± 0.72	:DME	
272	31	4.67	1991-Nov-19	7.38	0.90	3.53	6	5	10	11.56	2.50	1.94	$-1.72^{+1.30}_{-1.28}$	0.75	−2.00	3.15 ± 0.95	:DME	
277	9	1.74	1991-Nov-25	8.99	0.90	9.08	71	41	29	20.97	2.48	2.10	$0.22^{+0.12}_{-0.12}$	3.55	0.23	8.44 ± 1.14	DME	
277	22	1.74	1992-Jul-18	8.99	0.90	11.55	184	62	33	21.39	2.53	2.14	$0.71^{+0.08}_{-0.09}$	4.95	0.72	11.45 ± 1.26	DME	
277	23	1.74	1992-Jul-18	8.99	0.90	14.61	229	55	59	21.25	2.51	2.12	$0.69^{+0.07}_{-0.08}$	6.59	0.70	15.13 ± 1.47	DME	
290	1	1.46	1992-Jan-26	6.67	0.90	3.53	39	9	14	17.38	2.11	1.92	$0.30^{+0.24}_{-0.24}$	1.51	0.34	3.75 ± 0.90	DME	
205	1	4.31	1990-Jun-20	9.62	0.90	5.06	30	17	23	14.93	2.92	2.43	$1.40^{+0.32}_{-0.34}$	2.22	1.43	4.91 ± 0.87	MERG	0.710
211	539	3.95	1991-Feb-09	14.30	0.90	26.00	37	31	39	22.76	5.86	3.11	$-0.40^{+0.20}_{-0.23}$	2.09	−0.39	5.49 ± 0.82	MERG	0.000
212	32	1.19	1991-Mar-17	6.88	0.90	9.14	103	29	18	18.62	1.95	1.37	$1.44^{+0.14}_{-0.14}$	4.04	1.46	8.97 ± 1.44	MERG	0.923

Table 2 – *continued*

FID	SRC	N_H $\times10^{20}$	Date	Exposure ksec	Radius arcmin	f_x(orig) $\times10^{-14}$	C1	C2	C3	B1	B2	B3	α_{1d}	Norm$_{2d}$ $\times10^{-5}$	α_{2d}	f_x(fit) $\times10^{-14}$	Object Type	Redshift
220	33	3.94	1992-Apr-23	6.36	0.90	5.83	38	20	17	8.32	1.61	1.37	$0.28^{+0.17}_{-0.16}$	2.81	0.30	6.78 ± 1.26	MERG	0.000
226	27	1.19	1991-Jun-02	38.13	0.90	9.42	512	219	143	154.25	37.21	9.77	$0.45^{+0.07}_{-0.04}$	4.04	0.47	9.23 ± 0.61	MERG	0.000
252	31	0.78	1992-May-03	11.89	0.90	64.45	1129	249	333	44.36	5.38	3.28	$1.14^{+0.05}_{-0.02}$	28.85	1.15	64.16 ± 2.70	MERG	1.413
287	102	1.06	1992-May-31	7.92	0.90	10.43	99	43	31	17.64	2.46	1.44	$0.42^{+0.10}_{-0.11}$	4.32	0.43	9.06 ± 1.16	MERG	0.000
302	29	1.23	1992-Oct-03	10.04	0.90	5.10	52	17	19	27.43	2.69	1.53	$0.19^{+0.21}_{-0.20}$	2.05	0.22	4.99 ± 0.96	MERG	0.000
123	84	1.22	1991-Jun-04	19.89	0.90	3.24	102	32	24	51.71	8.00	4.34	$0.49^{+0.17}_{-0.15}$	1.16	0.51	2.77 ± 0.48	UNKN	
124	16	1.64	1991-Jun-28	13.65	0.90	3.10	86	30	26	51.44	13.93	4.83	$1.02^{+0.21}_{-0.25}$	1.50	1.05	3.35 ± 0.78	UNKN	
124	24	1.64	1991-Jun-28	13.65	0.90	3.16	84	27	16	48.93	13.25	4.60	$1.35^{+0.26}_{-0.25}$	0.94	1.40	1.95 ± 0.50	UNKN	
124	38	1.64	1991-Jun-14	13.65	0.90	5.58	103	21	45	43.07	11.67	4.05	$1.09^{+0.16}_{-0.17}$	3.04	1.11	6.54 ± 0.95	UNKN	
127	1	1.71	1991-Jun-15	20.21	0.90	3.43	89	31	37	53.98	9.76	6.17	$0.88^{+0.21}_{-0.22}$	1.54	0.90	3.62 ± 0.57	UNKN	
127	2	1.71	1991-Jun-15	20.21	0.90	3.65	77	35	32	53.58	9.69	6.12	$0.76^{+0.24}_{-0.24}$	1.76	0.78	4.14 ± 0.67	UNKN	
127	38	1.71	1991-Dec-04	20.21	0.90	3.63	77	34	42	56.83	10.28	6.49	$0.50^{+0.27}_{-0.28}$	1.71	0.51	3.99 ± 0.59	UNKN	
127	48	1.71	1991-Dec-04	20.21	0.90	3.23	121	35	28	54.35	9.83	6.21	$1.44^{+0.17}_{-0.16}$	1.33	1.47	2.93 ± 0.49	UNKN	
127	62	1.71	1991-Dec-04	20.21	0.90	3.39	109	31	26	54.02	9.77	6.17	$1.38^{+0.18}_{-0.19}$	1.14	1.41	2.47 ± 0.44	UNKN	
205	21	4.31	1991-Apr-10	9.62	0.66	5.01	12	11	28	8.01	1.57	1.30	$0.13^{+0.60}_{-0.77}$	2.22	0.10	5.52 ± 0.98	UNKN	
208	54	0.73	1991-Mar-08	15.22	0.90	3.50	64	18	30	36.38	3.48	2.53	$0.41^{+0.20}_{-0.24}$	1.61	0.43	3.83 ± 0.62	UNKN	
222	33	2.43	1992-Apr-01	12.89	0.90	3.56	36	12	22	26.64	3.36	2.54	$0.49^{+0.52}_{-0.69}$	1.71	0.52	4.09 ± 0.84	UNKN	
222	511	2.43	1992-Apr-01	12.89	0.90	6.00	63	25	45	29.71	3.75	2.83	$0.84^{+0.19}_{-0.22}$	2.88	0.85	6.70 ± 0.87	UNKN	
223	56	1.84	1990-Jun-21	36.12	0.90	6.32	209	68	94	108.65	8.31	4.86	$0.91^{+0.11}_{-0.12}$	2.88	0.92	6.44 ± 0.56	UNKN	
229	310	0.79	1991-Nov-10	12.29	0.90	3.10	33	12	19	34.46	3.53	2.38	$0.48^{+0.57}_{-0.79}$	1.07	0.51	2.94 ± 0.70	UNKN	
230	401	0.79	1991-Nov-10	18.78	0.90	3.25	158	28	32	59.02	7.80	3.93	$1.19^{+0.14}_{-0.13}$	1.48	1.21	3.14 ± 0.47	UNKN	
230	501	0.79	1991-Nov-10	18.78	0.90	5.00	76	16	13	57.47	7.60	3.82	$0.79^{+0.38}_{-0.43}$	0.52	0.85	1.25 ± 0.39	UNKN	
230	502	0.79	1991-Nov-10	18.78	0.78	5.00	61	17	7	46.20	6.11	3.07	$0.97^{+0.37}_{-0.46}$	0.36	1.06	0.82 ± 0.37	UNKN	
231	305	0.73	1991-Nov-12	10.89	0.90	5.45	55	21	37	33.94	5.85	3.49	$0.10^{+0.25}_{-0.26}$	2.53	0.11	6.14 ± 0.97	UNKN	
236	9	2.55	1991-Feb-23	4.95	0.90	3.05	12	6	12	10.71	1.59	1.10	$-0.07^{+0.83}_{-1.15}$	1.78	−0.12	4.70 ± 1.32	UNKN	
237	2	2.95	1991-Mar-15	6.37	0.90	5.99	35	10	30	15.31	1.89	1.75	$0.92^{+0.28}_{-0.33}$	3.56	0.95	8.25 ± 1.44	UNKN	
238	2	4.08	1991-Mar-15	7.65	0.90	5.86	16	21	21	14.90	4.22	1.94	$0.63^{+0.39}_{-0.51}$	2.59	0.65	6.05 ± 1.13	UNKN	
238	22	4.08	1991-May-22	7.65	0.90	3.50	16	6	15	13.62	3.86	1.78	$-0.82^{+1.49}_{-1.96}$	1.02	−1.56	3.77 ± 0.36	UNKN	
238	24	4.08	1991-Aug-24	7.65	0.90	4.04	16	10	14	13.69	3.88	1.79	$0.53^{+0.81}_{-1.13}$	1.57	0.53	3.71 ± 1.00	UNKN	
246	14	6.19	1991-Aug-01	22.47	0.90	4.97	60	29	58	37.84	8.01	6.04	$1.25^{+0.40}_{-0.63}$	2.34	1.27	5.23 ± 0.64	UNKN	
246	37	6.19	1991-Nov-14	22.47	0.90	4.85	43	37	45	36.58	7.75	5.84	$1.23^{+0.37}_{-0.42}$	2.07	1.24	4.63 ± 0.61	UNKN	
246	44	6.19	1991-Nov-14	22.47	0.90	3.48	60	30	44	39.18	8.30	6.25	$1.62^{+0.38}_{-0.42}$	1.72	1.64	3.93 ± 0.54	UNKN	
248	42	1.50	1992-May-12	19.55	0.90	5.53	49	34	41	47.68	7.57	4.42	$-0.09^{+0.30}_{-0.37}$	2.16	−0.08	5.38 ± 0.78	UNKN	
248	56	1.50	1992-May-12	19.55	0.90	4.37	71	32	41	52.37	8.31	4.85	$0.34^{+0.26}_{-0.28}$	1.74	0.35	4.12 ± 0.59	UNKN	
250	5	3.52	1992-May-12	19.37	0.90	4.12	32	25	37	28.15	3.57	3.65	$0.42^{+0.35}_{-0.45}$	1.99	0.43	4.69 ± 0.69	UNKN	
250	40	3.52	1991-Nov-14	19.37	0.60	3.04	19	8	42	14.65	1.86	1.90	$-1.68^{+0.96}_{-1.04}$	0.96	−1.94	3.90 ± 0.66	UNKN	
250	47	3.52	1991-Nov-14	19.37	0.90	6.81	21	26	76	31.97	4.05	4.15	$-0.92^{+0.46}_{-0.47}$	2.62	−0.95	7.89 ± 0.92	UNKN	
250	57	3.52	1991-Nov-14	19.37	0.48	3.03	9	14	16	8.73	1.11	1.13	$0.62^{+0.44}_{-0.53}$	1.27	0.64	3.00 ± 0.60	UNKN	
257	28	2.18	1991-Nov-26	11.47	0.90	5.00	19	7	36	17.12	3.51	2.01	$-2.24^{+1.24}_{-1.48}$	1.46	−3.00	8.15 ± 1.71	UNKN	
265	7	1.10	1991-Dec-13	12.02	0.90	6.35	37	22	48	35.69	4.24	3.38	$-0.63^{+0.37}_{-0.48}$	2.55	−0.64	7.11 ± 1.03	UNKN	
266	20	2.05	1992-Jan-15	8.34	0.90	3.12	42	12	13	23.40	3.51	2.68	$1.18^{+0.30}_{-0.35}$	1.26	1.24	2.66 ± 0.75	UNKN	

Table 2 – *continued*

FID	SRC	N_H $\times10^{20}$	Date	Exposure ksec	Radius arcmin	f_x(orig) $\times10^{-14}$	C1	C2	C3	B1	B2	B3	α_{1d}	Norm$_{2d}$ $\times10^{-5}$	α_{2d}	f_x(fit) $\times10^{-14}$	Object Type	Redshift
270	17	3.57	1992-Apr-09	8.08	0.90	3.09	26	7	13	27.52	9.36	2.51	$-1.84^{+1.62}_{-2.14}$	0.15	−5.63	2.57 ± 0.90	UNKN	
273	26	2.81	1991-Nov-25	5.17	0.90	4.42	27	12	13	10.61	2.98	1.36	$1.34^{+0.29}_{-0.31}$	2.44	1.40	5.23 ± 1.21	UNKN	
277	4	1.74	1991-Nov-25	8.99	0.90	3.20	39	9	15	20.92	2.47	2.09	$0.96^{+0.29}_{-0.36}$	1.27	1.00	2.97 ± 0.80	UNKN	
277	13	1.74	1992-Jul-18	8.99	0.72	3.03	15	5	17	13.32	1.57	1.33	$-0.92^{+1.04}_{-1.38}$	1.35	−1.29	4.62 ± 1.20	UNKN	
277	25	1.74	1992-Jan-27	8.99	0.90	3.41	66	15	21	21.17	2.50	2.12	$1.31^{+0.18}_{-0.19}$	1.97	1.34	4.21 ± 0.76	UNKN	
279	4	4.28	1992-Jan-27	7.64	0.90	7.29	59	16	25	33.46	3.98	1.87	$1.62^{+0.30}_{-0.33}$	2.92	1.66	6.65 ± 1.11	UNKN	
279	18	4.28	1992-Jul-08	7.64	0.90	5.48	35	15	16	31.99	3.81	1.79	$0.94^{+0.56}_{-0.70}$	2.42	0.97	5.49 ± 1.24	UNKN	
279	19	4.28	1992-Aug-31	7.64	0.90	7.21	81	19	16	31.64	3.77	1.77	$2.43^{+0.28}_{-0.15}$	2.62	2.54	7.10 ± 1.28	UNKN	
283	13	10.46	1992-May-12	6.15	0.90	7.42	19	8	15	8.52	1.76	2.19	$2.96^{+0.76}_{-1.22}$	2.38	3.10	4.60 ± 1.13	UNKN	
285	102	3.43	1992-May-17	8.19	0.90	3.40	8	7	8	7.94	1.72	1.72	$0.46^{+0.73}_{-1.09}$	1.12	0.49	2.77 ± 0.97	UNKN	
288	1	1.43	1992-May-09	6.77	0.90	3.64	42	9	9	17.10	1.56	1.37	$1.30^{+0.25}_{-0.28}$	1.22	1.36	2.50 ± 0.68	UNKN	
288	2	1.43	1992-May-09	6.77	0.42	4.68	32	7	17	4.40	0.40	0.35	$1.30^{+0.20}_{-0.20}$	2.53	1.33	5.36 ± 1.02	UNKN	
288	16	1.43	1992-Jan-26	6.77	0.90	4.21	38	10	14	16.97	1.55	1.36	$0.98^{+0.26}_{-0.27}$	2.27	1.02	5.28 ± 1.41	UNKN	
288	19	1.43	1992-Jan-26	6.77	0.90	3.60	40	14	7	17.36	1.58	1.39	$1.26^{+0.27}_{-0.25}$	1.67	1.32	3.42 ± 0.89	UNKN	
292	12	3.48	1992-Apr-02	7.09	0.90	3.34	14	14	8	15.13	3.89	1.80	$0.74^{+0.55}_{-0.79}$	1.15	0.79	2.65 ± 0.87	UNKN	
299	105	1.56	1992-Oct-03	8.01	0.90	4.89	120	15	19	24.55	5.84	4.48	$1.90^{+0.26}_{-0.11}$	1.64	2.01	3.94 ± 0.89	UNKN	
303	108	3.55	1992-Nov-13	9.96	0.90	5.29	37	20	31	22.41	3.35	4.31	$0.96^{+0.33}_{-0.35}$	2.72	0.99	6.19 ± 1.06	UNKN	
303	112	3.55	1992-Nov-13	9.96	0.90	4.12	30	13	16	21.76	3.25	4.19	$1.15^{+0.46}_{-0.60}$	1.58	1.21	3.54 ± 0.92	UNKN	
304	25	3.56	1992-Nov-13	17.73	0.90	7.18	23	49	67	26.39	3.66	3.87	$0.12^{+0.25}_{-0.27}$	3.38	0.12	8.12 ± 0.85	UNKN	
304	26	3.56	1992-Oct-28	17.73	0.90	3.24	34	20	30	26.28	3.64	3.85	$0.64^{+0.40}_{-0.48}$	1.42	0.66	3.30 ± 0.56	UNKN	

Columns 1 and 2 give the field ID and source ID for each source (see Mason et al., in preparation, for details). Column 3 is the N_H in atom cm^{-2}. Column 4 is the observation date. Column 5 is the exposure time of the field in ks. Column 6 is the extraction radius for the source counts. Column 7 is the original flux (0.5–2 keV) derived by assuming an absorbed power law of slope 1. Columns 8–10 are the extracted total counts in each band. Columns 11–13 are the extimated background counts within the extraction circle for each band. Column 14 is the marginalized power-law slope. Column 15 is the normalization of the best fit (in units of photon keV^{-1} cm^{-2} s^{-1}) and column 16 is the best-fitting slope. Column 17 is the flux (0.5–2 keV) determined from the best-fitting data. Column 18 is the object type. Column 19 is the redshift (if applicable). For both columns 18 and 19 a colon indicates that either the identification or the redshift is uncertain.

UK Deep Survey show that the fraction of quasars at very faint flux levels declines, but that of NELGs rapidly increases (McHardy et al. 1999). Extrapolations to zero flux indicate that up to 50 per cent of the X-ray background may be due to NELGs. The spectral shape of NELGs is therefore of crucial importance if we are to understand the nature of the soft X-ray background. However, a fundamental problem with this class of object is that the term NELG is a nebulous categorization. They include hidden AGN, such as Seyfert 2 galaxies where the emission is likely to be non-thermal and absorbed, to starburst galaxies and H II region galaxies, where the emission is thought to be thermal in nature and arising from shocked gas with a typical temperature of 0.5–1 keV. From our work on stars, we know that we can distinguish between thermal and non-thermal sources on the basis of the fits to the three-colour data, so we should be able to estimate the ratio of thermal to non-thermal sources in the RIXOS sample.

There are 18 NELGs in RIXOS identified on the basis of their optical spectra. Fig. 12 shows the distribution of observed minus predicted counts for the NELGs. In general, the NELGs seem consistent with a power law, with only one source (122-16) showing a significant deviation in all three bands. This may imply thermal emission from this object, although preliminary studies of higher resolution data from 122-16 indicates that the X-ray spectrum is complex. Fig. 14 shows the estimated mean slope and dispersion of the NELGs in comparison with the AGN, and Fig. 13 shows the power-law slope as a function of redshift. This demonstrates no clear evidence for spectral evolution with redshift. Fig. 13 does show that there is a large range of potential slopes, with some of the sources being very hard. At least one of these hard sources has been identified with a Seyfert 2 galaxy, which is entirely consistent with the flat spectral slope.

Thus the X-ray spectra of NELGs in the RIXOS sample are indistinguishable from those of the AGN. This is consistent with the fact that high-resolution optical data on X-ray-selected NELGs have shown that many objects classified as NELGs on the basis of low signal-to-noise data have broad components to the permitted lines (e.g. Boyle et al. 1995), and at least two H II region-like galaxies have been observed to show strong X-ray variability more consistent with that seen in AGN (Boller, Fink & Schaeidt 1994; Bade, Komossa & Dahlem 1996). Further, HRI images of low-luminosity AGN show that the X-ray emission is mostly nuclear, again supporting the idea that the origin of the X-ray emission is nuclear in nature (Koratkar et al. 1995). Thus many objects classified as NELGs above the RIXOS flux limit may contain active nuclei.

However, it is important to note that the average slope that we find for the RIXOS NELGs is inconsistent with the average slope of a sample of much fainter NELGs from the UK Deep Field (Romero-Colmenero et al. 1996). In the latter study the average slope was $\alpha = 0.45 \pm 0.09$, a value that is more consistent with the average slope of the RIXOS clusters. There is clearly a discrepancy between the average properties of NELGs in the RIXOS sample and those found at much fainter fluxes, which may imply some difference in the type of objects seen at the faintest fluxes. Another possibility is that there are more absorbed sources in the fainter samples, which would pull down the average slope. Without higher resolution data and good signal-to-noise ratios it is impossible to distinguish between these two possibilities.

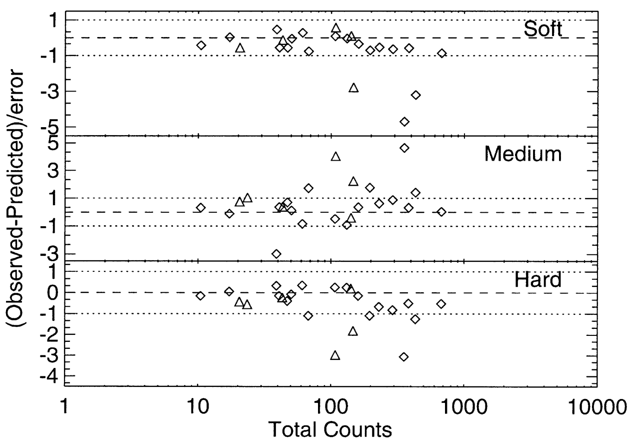

Figure 12. The predicted minus observed counts for the NELGs (◇) and isolated galaxies (△). The dotted lines denote 1σ around zero.

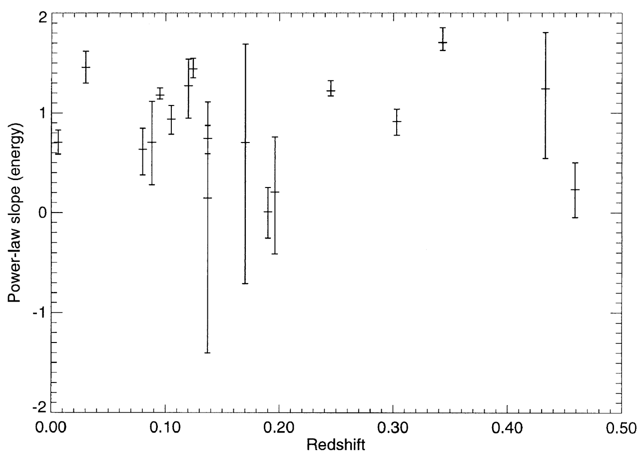

Figure 13. The fitted power-law slope versus the redshift for the NELGs in the RIXOS sample. No evolution of the power-law slope can be seen.

6.4 The AGN

By far the largest fraction of objects in the RIXOS sample have been classified as AGN. Unlike the stars and clusters of galaxies, a non-thermal model such as a power law is likely to be an acceptable fit to the data, although in detail more complex models

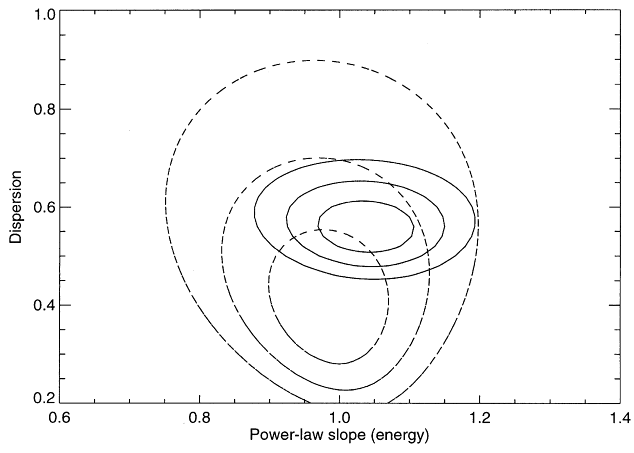

Figure 14. The values of the slope and dispersion for the RIXOS AGN (solid line) and the NELGs (dashed line). It is clear that the two samples are indistinguishable.

may be appropriate (e.g. Nandra & Pounds 1994). Fig. 14 shows the mean slope and dispersion for the RIXOS AGN; we find $\alpha = 1.05 \pm 0.05$ and an intrinsic scatter of 0.55 ± 0.05. These numbers are slightly steeper than those found for the EMSS AGN (0.9 ± 0.05 with a dispersion of 0.35 ± 0.04), which sampled a harder energy range (0.3–4 keV) than the PSPC. However, this is much flatter than the slopes found for bright, nearby Seyferts observed with *ROSAT* (e.g. Walter & Fink 1993; Fiore et al. 1994; Laor et al. 1994), and is also flatter than the average slope found for the fainter AGN contained in the CCRS ($\alpha = 1.3 \pm 0.1$; Ciliegi et al. 1997). A slope of $\alpha = 1$ is, however, consistent with what is believed to be the underlying power-law slope in nearby Seyferts (e.g. Nandra & Pounds 1994).

6.4.1 Goodness of fit for a power law

Fig. 15 shows the predicted minus observed total counts expressed in terms of the standard deviation for each spectral band for all the AGN. It is clear that for the majority of AGN a power-law fit is a reasonable representation of the spectral shape, as most of the data points lie within one sigma of the model. However, there do seem to be a number of AGN where the observed counts are significantly underestimated in the medium band. It is not clear what causes this deviation, as these sources seem to contain a mixture of slopes ranging from soft to hard. One possibility is that some contain a significant O VII edge, implying the presence of a warm absorber. However, three-colour data are not sufficient to determine the origin of this deviation, and higher resolution data are required. We have extracted high-resolution data for the source with the largest discrepancy in the soft band, source 258-001, which is sufficiently bright to warrant this. Analysis of these data shows evidence for an edge at 1.1 keV, which has been tentatively identified with silicon (Mittaz et al., in preparation). The ability to detect such a source shows the power of fitting three colours to reveal peculiar features. From Fig. 15 approximately 20 per cent of sources appear to be deviant from a power-law model.

Without analysing all of the data at higher resolution, it is difficult to make strong claims about objects where a simple power-law does not appear to be an adequate description of the data. As noted in Section 4, within the sample there are a number of sources which deviate significantly from the average spectrum. For example, some AGN have positive slopes, which correspond to those in the $C1 < 0$ region of the colour–colour diagram. Such objects may be intrinsically absorbed, and one (278-010) has sufficient counts to allow us to extract a higher resolution spectrum. On the assumption that the absorbing column is at the Stark et al. (1992) value of $1.94 \times 10^{20}\,\mathrm{cm}^2$, a fit to these higher resolution data gives a slope of $\alpha = -1.17 \pm 0.2$, consistent with the value fitted to the three-colour data. However, if we fit an intrinsic column in addition to the Galactic N_{H}, we detect an instrinsic column at > 90 per cent confidence with a fitted power-law slope of $\alpha = (1.4^{+2.3}_{-1.7})$ and a best-fitting intrinsic N_{H} of $(6^{+6}_{-4}) \times 10^{21}\,\mathrm{cm}^{-2}$ (68 per cent confidence limits). Fig. 16 shows the 68, 90 and 99 per cent contours of the intrinsic absorption plotted against power-law slope. On the assumption that this holds true for the other AGN with $C1 < 0$, we can conclude that ~5 per cent of the RIXOS AGN sample show detectable amounts of intrinsic absorption. We note that trends between the fitted X-ray and optical spectral slopes, and between the X-ray spectral slope and the ratio of X-ray to optical flux, of RIXOS AGN have also be interpreted as being due to the effects of absorption (Puchnarewicz et al. 1996).

From the fitted power-law slopes it is moreover clear that there are not only hard sources, but also those which have slopes significantly steeper than $\alpha = 1$. We have taken the object with the steepest slope that has a sufficiently large number of counts (227-301), and have extracted higher resolution X-ray data for it. A single power law gives a very bad fit, with a χ^2_ν of 6.8. We therefore fitted the data with a power-law and blackbody model (to represent any soft excess), and the fit improved dramatically, with a χ^2_ν of 0.56. The best-fitting parameters give a power-law slope of $\alpha = 0.7 \pm 0.7$ (68 per cent) and a black-body temperature of 0.0085 ± 0.001 keV (68 per cent) (Fig. 17). The value of the power-law slope is now consistent with the average for the RIXOS AGN, and the black-body component has a similar temperature to that seen the USS sample (Thompson & Cordova 1994). It is therefore clear that RIXOS contains a range of objects, from intrinsically absorbed AGN and those with strong soft excesses to objects with absorption edges. The high-resolution data show that fits to the three-colour data can give sufficient information to separate out those objects which have non-standard X-ray spectra.

6.4.2 Spectral evolution

A further question of interest is whether there is any evolution of the X-ray spectral slope of AGN with redshift. The nature of any

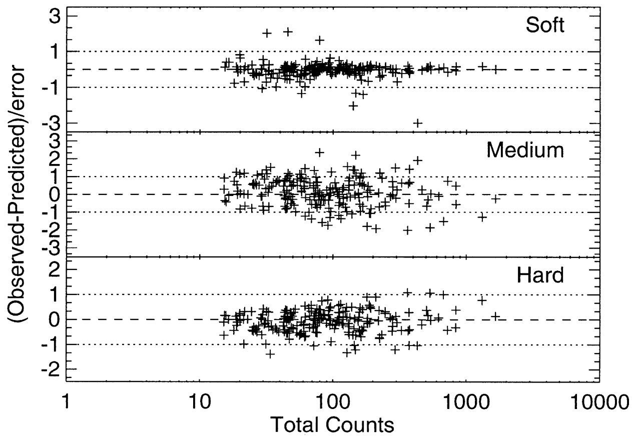

Figure 15. The predicted minus observed counts for the AGN. The dotted lines denote 1σ around zero.

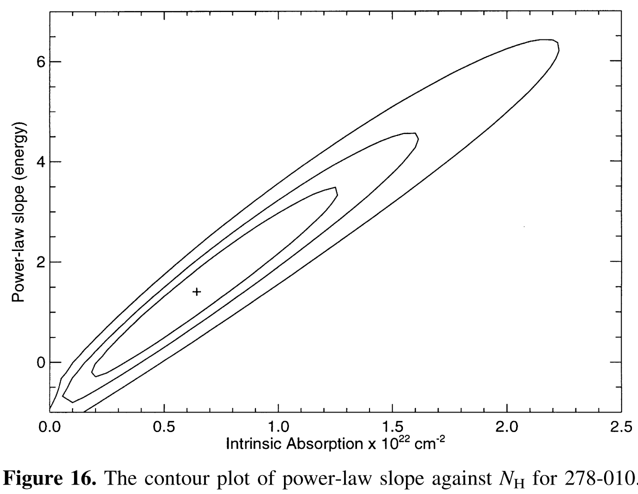

Figure 16. The contour plot of power-law slope against N_{H} for 278-010. Intrinsic absorption can be clearly seen.

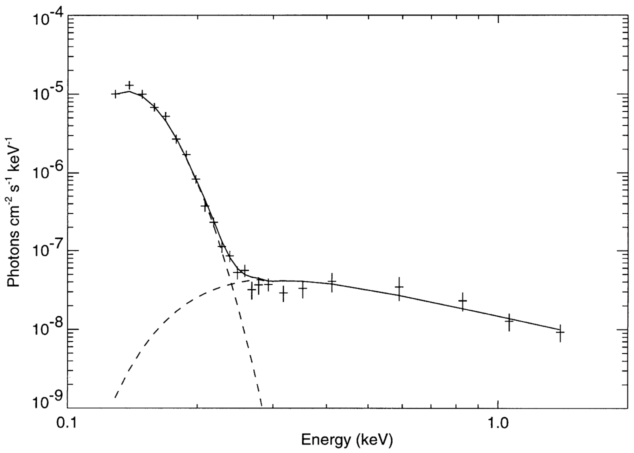

Figure 17. A multicomponent fit to the X-ray spectrum of 227-301. The best-fitting model (blackbody and power-law) is shown.

such spectral evolution has consequences for both our understanding of the X-ray-emitting process and the nature of the X-ray background. Fig. 18 shows the distribution of slopes as a function of redshift, where we have used variously sized redshift bins. It is apparent from Fig. 18 that there is no evidence for any spectral evolution at all. This lack of evolution in the spectral slopes is consistent with the results of other similar samples (e.g. Ciliegi et al. 1997). To investigate this further, we have recalculated the intrinsic slope and dispersion for AGN below and above a redshift of 1, where we have approximately equal numbers of AGN in each of the two bins. From Fig. 19 it is clear that the slopes and dispersions are effectively identical for objects above and below the redshift divide. As noted by Ciliegi et al., the fact that there is no apparent spectral evolution implies that the power-law spectrum in the AGN rest frame extends from soft X-rays out to at least 8 keV with the same slope. This excludes models with strong or hot soft excesses as being typical of AGN in the RIXOS sample.

6.4.3 *Interpretation and comparison with other surveys*

The standard model for the X-ray emission from AGN derived from missions previous to *Ginga* and *ROSAT* was one of a medium-energy power law with a slope of $\alpha = 0.7$, with many objects showing evidence for a soft X-ray excess. Such an excess is normally assumed to be due to the high-energy tail of an accretion disc spectrum (e.g. Turner & Pounds 1988). However, with the advent of *ROSAT* and more recently *ASCA*, the situation has been found to be more complex. In detail it is often necessary to use models including reflection and warm absorbers as well as simple power laws (e.g. Nandra & Pounds 1994). Approximately 50 per cent of nearby Seyferts studied by *Ginga* have shown some evidence for warm absorbers, and evidence for an absorption line at 0.7 keV identified as O VII has even been found in PSPC data alone (e.g. Nandra & Pounds 1992).

Over the past decade there has been a lot of work on soft X-ray surveys of AGN, and a number of samples have been compiled. The largest of these is the EMSS (Gioia et al. 1990), which consists of 421 AGN detected in the 0.5–4.5 keV band. Maccacaro et al. (1988) found a mean spectral index for the AGN of $\alpha = 1.03 \pm 0.05$ with a dispersion of $\sigma = 0.36$. Later surveys indicated that there may be an average steepening of the spectrum

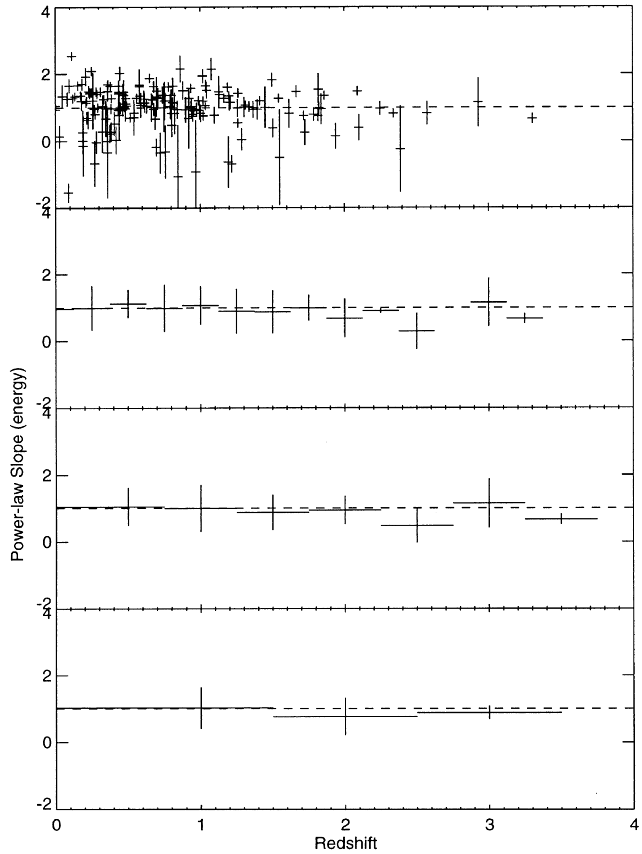

Figure 18. Fitted slopes for the RIXOS AGN as a function of redshift. Each panel shows the data binned into successively bigger redshift bins, with the error bar representing the rms scatter about the mean, and shows that there is no evolution in the spectral slope. In the case of the middle two panels, the last two data points contain a single object, and the plotted error is simply the error on the fit to those objects.

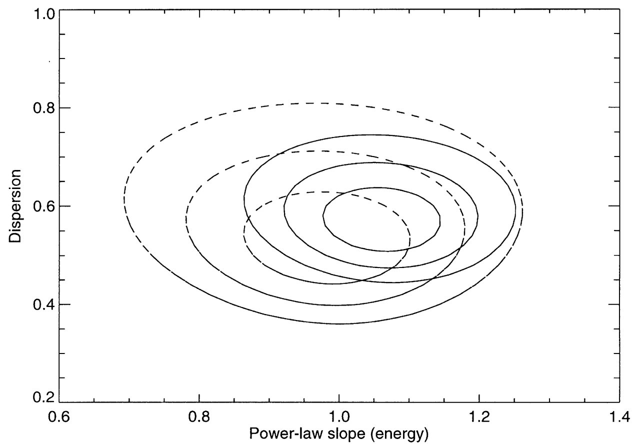

Figure 19. Intrinsic slope and dispersion for the RIXOS AGN separated into objects above and below a redshift of 1. It is clear that the two samples are identical, implying no strong evolution in the spectral parameters of the AGN.

towards softer energies. The Ultra-Soft Survey from *Einstein* showed that AGN selected below 0.5 keV have an average slope of $\alpha = 1.45$ (Thompson & Cordova 1994). The *EXOSAT* High Galactic Latitude Survey (HGLS), which covered the energy range 0.2–2 keV, was consistent with a mean spectral slope of

$\alpha = 1.3$ (Giommi et al. 1991), and work on *ROSAT* PSPC observations has indicated that the average spectrum of nearby bright AGN is about $\alpha = 1.5$ (e.g. Walter & Fink 1993). Recently, Schartel et al. (1996) used the *ROSAT* all-sky survey data for the QSOs in the Large Bright QSO Survey, and found a mean energy index of $\alpha = 1.70 \pm 0.2$ for the radio-quiet QSOs. Moving to higher redshift samples, Bechtold et al. (1994) found $\alpha = 1.15 \pm 0.14$ for a sample of high-redshift, radio-quiet quasars, and Reimers et al. (1995) found $\alpha = 1.25 \pm 0.2$ for another high-redshift sample. It is difficult to make general statements on the basis of these different samples, however, since each has its own selection criteria and may therefore sample different populations of sources.

None of the above samples is directly comparable to RIXOS, either because they are optically selected, or because they select bright X-ray sources, both of which can favour AGN with soft X-ray spectra (Puchnarewicz et al. 1996). There are, however, *ROSAT* serendipitous surveys with which a direct comparison should be more meaningful, although none are as large and/or complete as RIXOS. The CCRS, which has a similar flux limit to RIXOS, has a reported average slope which lies between the EMSS average and the average for the brighter samples, with $\alpha = 1.3 \pm 0.1$ (Ciliegi et al. 1997). At the very faintest fluxes, the average spectral slopes for QSOs in the UK Deep Survey is $\alpha = 0.96 \pm 0.03$ (Romero-Colmenero et al. 1996), which is consistent with the EMSS. The spectrum of the QSOs in another deep survey has an average of $\alpha = 1.23 \pm 0.04$ (Almaini et al. 1996). Both the Ciliegi et al. and the Almaini et al. samples are therefore softer than the RIXOS average of $\alpha = 1.05 \pm 0.05$.

The largest difference is between the CCRS sample and RIXOS. Although the discrepancy is only at the 2σ level, it would be expected that these two samples would give essentially identical results, as the flux limits for the CCRS are only slightly lower than for RIXOS. However, the analysis techniques are different. From the simulations described in Section 5.3 it would be expected that the hardness-ratio method used in the CCRS would give an average slope that was slightly softer than the 'true' value. We have attempted to re-analyse the CCRS data using the method used for the RIXOS sample. However, because accurate positions are not quoted for sources in the CCRS, it has not been possible to analyse the CCRS in exactly the same way as for RIXOS, since we cannot unambiguously identify all the X-ray sources. Nevertheless, Fig. 20 shows the comparison between the RIXOS sample and our best estimate for the CCRS sample analysed using the Cash method, and the discrepancy between the two is reduced. The revised average slope of the CCRS, 1.16 ± 0.1, is now consistent with the RIXOS sample at 1σ, implying that the apparent difference between the two samples was caused at least in part by the bias introduced by using hardness ratios. The difference between the two dispersion estimates is likely to be caused by the assumption of a Gaussian distribution of slopes rather than necessarily representing a real difference between the two samples.

From the range of different slopes obtained from different samples it is clear that the spectral distribution of AGN is quite complex, and that source selection effects can play a dominant role in determining the average slope within a given sample. Nevertheless, the evidence increasingly suggests that faint, X-ray-selected AGN, such as those found in *ROSAT* serendipitous surveys, have a mean slope close to $\alpha = 1$. Such an index is close to the value estimated to be the underlying intrinsic X-ray spectrum in Seyferts when effects such as reflection and a warm

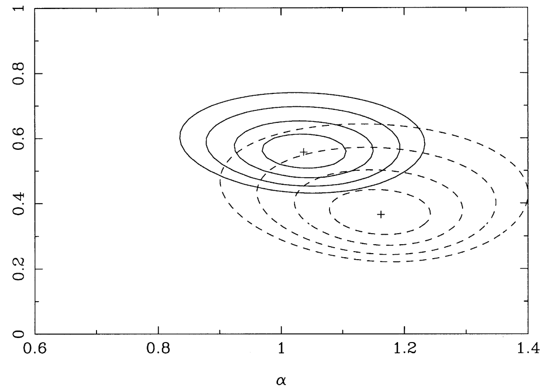

Figure 20. A comparison of the RIXOS average slope and dispersion for the AGN (solid contour) and the estimated spectral slope and dispersion for the CCRS (dashed contour). Both contours have been obtained in precisely the same way, using the Cash statistic.

absorber are taken into account (Nandra & Pounds 1994). It is also close to the value of the inferred spectral slope seen in the IR, giving rise to claims that there is a power law of energy index 1 underlying the observed spectrum from the IR to X-ray range (e.g. Elvis et al. 1986). Deviations from this average slope can then be caused by additional processes such as soft X-ray excesses, warm absorbers and reflection, the effects of which are likely to be a function of redshift and/or luminosity. Some of these additional effects have already been observed in some high-redshift objects. For example, warm absorbers have been detected so far in two quasars, 3C 351 (Fiore et al. 1993) and MR 2251−178 (Pan, Stewart & Pounds 1990) though it is unclear how prevalent they are. However, without a detailed study of objects contained within RIXOS and other similar samples it is not possible to determine the proportion of objects in which these extra effects are important.

One final question needs to be addressed, and that is the effect of intrinsic absorption. Observations of selected high-redshift quasars have indicated that absorption may be important in some objects (Elvis et al. 1994). High-resolution spectra of CCRS AGN with sufficient counts to determine $N_{\rm H}$ show only one object out of 36 AGN with evidence for significant absorption (Ciliegi et al. 1997), while in the data of Almaini et al. (1996) two out of nine objects require extra absorption. Selection effects may be at work here, since a source that is absorbed will appear fainter than the same source that is not, and the constraints on spectral fits are obviously better for brighter sources. However, from the X-ray colour–colour data there are indications that at least ~5 per cent of the RIXOS AGN have detectable absorption based on the X-ray data alone. This fraction is fairly secure, because even at the flux cut-off of $3 \times 10^{-14}\,{\rm erg\,cm^{-2}\,s^{-1}}$ RIXOS sources contain significant numbers counts. This is confirmed by simulations. We have constructed 1000 data sets with the same flux distribution and assumed slope distribution ($\alpha = 1$ and $\sigma = 0.55$) as the RIXOS sample, and have analysed these data sets in exactly the same way as discussed in Section 4. Out of the 1000 simulated data sets, only one of the simulated data sets has as many AGN in the $C1 < 0$ region of the colour–colour plot as are actually seen, as illustrated in Fig. 21.

Even in those samples with much lower flux limits than exist in the RIXOS samples there is no evidence for extra absorption being required for the majority of the QSO part of the sample. Therefore, based on the X-ray data alone, there is no strong evidence for absorption playing a major role in the X-ray spectra of faint AGN, and such effects exist only at the ~10 per cent level.

7 ANALYSIS OF THE WHOLE RIXOS SAMPLE

Finally, we have analysed the whole RIXOS sample, including all sources in all RIXOS fields down to the detection limit of each field, containing 1762 sources. Even though we do not have identifications for most of the sources with a flux below 3×10^{-14} erg cm^{-2} s^{-1}, we can still study the spectral shape of the faintest sources, which are precisely those which will contribute most to the soft X-ray background. Recent work has indicated that there may be a correlation between the average spectral slope and flux (Hasinger et al. 1993; Vikhlinin et al. 1995). Vikhlinin et al. (1995) analysed 130 *ROSAT* fields and extracted average spectra over a range of flux bins. They showed a correlation between source flux and spectral index, with bright sources ($>2 \times 10^{-13}$ erg cm^{-2} s^{-1}) having average slopes close to 1.3, and faint sources ($<10^{-14}$ erg cm^{-2} s^{-1}) having average slopes close to 0.5. As noted by Vikhlinin et al., the average slope of 0.5 is close to that obtained for the soft X-ray background.

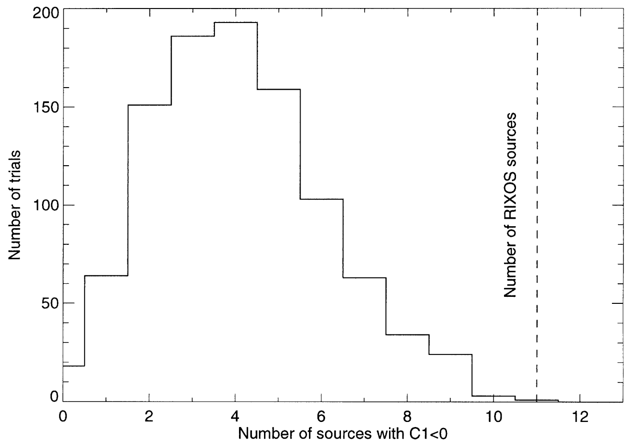

Figure 21. A histogram showing the number of times a given number of hard ($C1 < 0$) sources were found in simulated samples of RIXOS AGN. The simulated samples have the same flux and spectral distribution as the RIXOS AGN, with a mean $\alpha = 1$ and dispersion $\sigma = 0.55$. Only one of the simulated data sets have as many hard sources as were seen in the RIXOS sample of AGN.

The exact significance of this correlation is, however, unclear, since Vikhlinin et al. used either hardness ratios, which in the case of the faintest sources will have a bias to softer slopes (see Section 5.3), or summed up all the sources in a flux bin and fitted multichannel data with models using χ^2. While summing up the data will allow higher signal-to-noise ratios at a higher resolution, it can only give information on the average properties of the sources and not on the distribution of slopes in a given flux band.

By using the Cash statistic technique on three-colour data we can avoid problems of biases. We have analysed the whole RIXOS sample containing 1762 sources, including sources which extend down to a flux of 4×10^{-15} erg cm^{-2} s^{-1}. Fig. 22 shows the fits to the whole sample as a function of flux both as a scatter plot and binned into flux bins. The second panel shows the average of the slopes in each flux bin which is the equivalent of the Vikhlinin et al. data. As with the sample of Vihklinin et al., there is a clear trend towards harder spectra at lower flux limits in the latter. Above the RIXOS flux limit there is no significant hardening, while there is a significant deviation below $\sim 2 \times 10^{-14}$ erg cm^{-2} s^{-1}. However, unlike the Vihklinin et al. sample we can

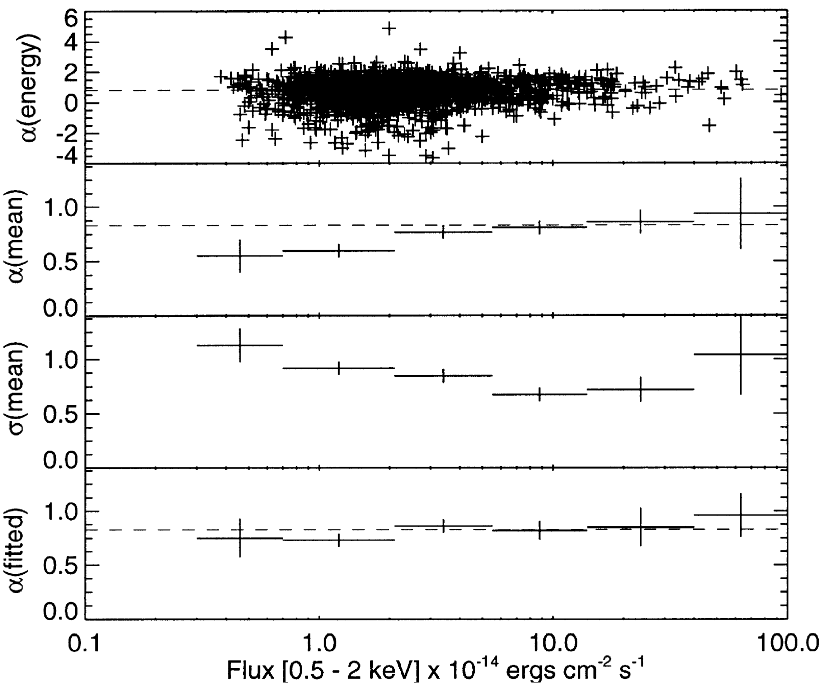

Figure 22. Fits to the whole RIXOS data set, consisting of 1762 objects. The top panel shows the power-law slope fit to all the data assuming Galactic N_H. The second panel shows the data averaged in 6 flux bins, together with the standard error. A clear trend can be seen, with the average hardening with lower fluxes. The third panel shows the standard deviation of the data around the mean. The bottom panel shows the fitted average slope and error in each flux bin. This method essentially biases against extreme outliers, and is more representative of the mode of the distribution. These data show no strong correlation with flux. In all cases the dashed line is representative of the mode of the slopes.

look at the distribution of slopes within a flux bin. The top panel of Fig. 22 makes it clear that the majority of sources do not show a trend to harder slopes at lower flux limits. To highlight this further, we have fitted the mean slope and dispersion within each flux bin in the same way as we have done for the RIXOS sample (Section 6). The bottom panel shows the fitted average slope as a function of flux, and it is clear that there is no significant trend. The most obvious explanation for this discrepancy between the arithmetically averaged data and the fitted average value is that there are changes in the distribution of slopes within a flux bin rather than a global change in the spectral slope. This is supported by the third panel, which shows an increase in the measured standard deviation of the data with decreasing flux. In the RIXOS data it is clear that there are a number of very hard sources below a flux of $3\times10^{-14}\,\mathrm{erg\,cm^{-2}\,s^{-1}}$. These sources would bias the mean but, as outliers, they would not have a significant effect on fits of a Gaussian distribution to the slopes, exactly as observed. If we look at those sources where $\alpha<0$, then 20 per cent of sources below $3\times10^{-14}\,\mathrm{erg\,cm^{-2}\,s^{-1}}$ satisfy this condition. However, if we look at all those sources with fluxes greater than $3\times10^{-14}\,\mathrm{erg\,cm^{-2}\,s^{-1}}$, then only 13 per cent of the sources satisfy this criterion. It is therefore clear that as we go to fainter fluxes a higher proportion of the sources are very hard. From studies of deep *ROSAT* pointings it is unlikely that there are a significant number of stars at faint fluxes, and it is more likely that the sources with hard spectra are an absorbed population. One obvious candidate for these sources are Seyfert 2 galaxies. Such sources are both hard and faint relative to unobscured AGN, and would therefore give the observed distribution which has more hard sources at fainter fluxes.

7.1 The nature of the soft X-ray background

One question that has been highlighted by recent *ROSAT* observations is the nature of the soft X-ray background. It has been known for many years that the average slope of the soft X-ray background is $\alpha=0.4$ (for a review see Fabian & Barcons 1992). This spectrum is inconsistent with the average spectrum of (relatively bright) AGN. From the deepest surveys undertaken to date it is clear that a significant fraction of the X-ray background is made up of emission from NELGs, an amorphous classification that may include Seyfert 2 galaxies as well as starburst galaxies and LINERS. However, the average spectrum of the RIXOS NELGs is also too soft to explain the soft X-ray background.

In contrast, the mean spectrum of NELGs at fainter flux levels *is* consistent with the X-ray background (Romero-Colmenero et al. 1996), and harder than that of AGN even in the same flux range. In the previous section we showed that the hard overall mean spectrum at faint fluxes is caused by a population of very hard sources (i.e., harder than the background). These bias the mean source spectral slope to a value which is consistent with the slope of the background.

A combination of two possible explanations may account for the slope of the X-ray background, given that the NELGs are likely to be a mixture of intrinsic source types. There may be a genuine change in the dominant emission mechanism between the bright RIXOS NELGs and those identified in deep surveys, with the emission from faint NELGs being dominated by a hot continuum source (e.g., hot gas, perhaps associated with an extended halo rather than the galactic nucleus); or the very hard sources which we identify in the extended RIXOS sample may be an absorbed population consisting, say, of Seyfert 2 galaxies (cf. Grindlay & Luke 1990). More sensitive individual X-ray spectral observations of a sample of faint sources will be needed to resolve this question.

8 CONCLUSIONS

RIXOS is a flux-limited, nearly complete sample of X-ray-selected sources. We have demonstrated that for such a sample it is possible to obtain useful spectral information even down to very faint limits, as long as the correct statistic is used. In contrast, a simple hardness-ratio method, which has been used by a number of authors to determine the spectral slope for faint sources, is shown to bias in the inferred power-law slope towards a steeper spectrum. The use of three-colour data allows some discrimination between thermal and non-thermal X-ray emission, at least for relatively bright sources. We have determined the spectral characteristics for each subcategory of sources within the RIXOS survey.

(1) Although little can be said directly about the X-ray spectra of the stars, the use of three-colour data demonstrates the ability of the method to discriminate between thermal and non-thermal sources.

(2) Most of the RIXOS clusters are consistent with the majority of the emission arising from hot ($>3\,\mathrm{keV}$) gas. There are some clusters where there is evidence for a lower temperature, which may indicate the presence of a cooling flow.

(3) On average, the NELGs have X-ray spectra that are consistent with the spectra of the AGN and may indicate that many of the NELGs found in RIXOS are, in fact, low-luminosity AGN. This is at variance with the X-ray spectra of NELGs found from deep X-ray surveys, where the average slope is much harder. The NELGs observed in deep X-ray surveys are then either a more absorbed population of sources, or the X-ray emission in the faintest NELGs arises from some mechanism other than an AGN non-thermal power law.

(4) The AGN have an average slope of $\alpha=1.05\pm0.05$, with no evidence for spectral evolution. This average slope is somewhat harder than the averages found for other samples of soft X-ray-selected AGN. However, the inappropriate use of hardness ratios will have softened the average slopes in other samples. The value of $\alpha=1.05$ is consistent with the naked power-law expected from AGN, implying that the X-ray spectrum of the RIXOS AGN is relatively uncontaminated by processes such as reflection and absorption. Since many of the previous X-ray-selected samples concentrated on low redshift/low luminosity AGN, part of the discrepancy between RIXOS and other samples may be ascribed to the effect of redshift and/or luminosity on the processes that modify the underlying power law.

(5) Analysis of the whole RIXOS sample confirms the presence of a flux dependent spectral slope (Hasinger et al. 1993; Vikhlinin et al. 1995). However, we have been able to investigate the cause of this correlation, and the most likely explanation is of an increasing proportion of very hard sources rather than an average hardening of the spectra.

ACKNOWLEDGMENTS

We thank all the RIXOS team for their work in obtaining and reducing the data. We also thank Liz Puchnarewicz for checking the source count extraction procedure. FJC thanks the DGES for parcial financial support, under project PB95-0122. HA benefited from financial support by CONACYT (Mexico; Cátedra Patrimonial, ref 950093). The RIXOS project has been made possible by the award of International Time on the La Palma telescopes by the Comité Científico Internacional. This research has made use of data obtained from the UK *ROSAT* Data Archive Centre at the Department of Physics and Astronomy, University of Leicester (LEDAS). We thank the Royal Society for a grant to purchase equipment essential to the RIXOS project.

REFERENCES

Almaini O., Shanks T., Boyle B. J., Griffiths R. E., Roche N., Stewart G. C., Georgantopoulos I., 1996, MNRAS, 282, 295

Bade N., Komossa, S., Dahlem, M., 1996, A&A, 309, 35L

Bechtold J. et al., 1994, AJ, 108, 759

Boller T., Fink H., Schaeidt S., 1994, A&A, 291, 403

Bowyer S., Lieu R., Lampton M., Lewis J., Wu X., Drake J. J., Malina R., 1994, ApJS, 93, 569

Boyle B. J., Shanks T., Georgantopoulos I., Stuart G. C., Griffiths R. E., 1994, MNRAS, 271, 639

Boyle B. J., McMahon R. G., Wilkes B. J., Elvis M., 1995, MNRAS, 272, 462

Branduardi-Raymont G. et al., 1994, MNRAS, 270, 947

Carballo R., Warwick R. S., Barcons X., Gonzalez-Serrano J. I., Barber C. R., Martinez-Gonzalez E., Perez-Fownon I., Burgos J., 1995, MNRAS, 277, 1312

Carrera F. J., Barcons X., Fabian A. C., Hasinger G., Mason K. O., McMahon R. G., Mittaz J. P. D., Page M. J., 1998, MNRAS, 299, 229

Cash J., 1979, ApJ, 228, 939

Castander F. J. et al., 1995, Nat, 377, 39

Ciliegi P., Elvis M., Wilkes B. J., Boyle B. J., McMahon R. G., 1997, MNRAS, 284, 401

Elvis M., Green R. F., Bechtold J., Schmidt M., Neugebauer G., Soifer B. T., Mathews K., Fabbiano G., 1986, ApJ, 310, 291

Fabian A. C., Barcons X., 1992, ARA&A, 30, 429

Fiore F., Elvis M., Mathur M., Wilkes B. J., McDowell J. C., 1993, ApJ, 415, 129

Fiore F., Elvis M., McDowell J. C., Siemiginowska A., Wilkes B. J., 1994, ApJ, 431, 515

Gioia I. M., Maccacaro T., Schild R. E., Wolter A., Stocke J. T., Morris S. L., Henry J. P., 1990, ApJS, 72, 567

Giommi P. et al., 1991, ApJ, 378, 77

Grindlay J. E., Luke M., 1990, Gorenstein, Zombeck, eds, High resolution X-ray Spectroscopy of Cosmic Plasmas. Cambridge Univ. Press, Cambridge, p. 276

Hasinger G., Burg R., Giacconi R., Hartner G., Schmidt M., Trumper J., Zamorani G., 1993, A&A, 275, 1

Koratkar A., Deustua S. E., Heckman T., Filippenko A. V., Ho L. C., Rao M., 1995, ApJ, 440, 132

Laor A., Fiore F., Elvis M., Wilkes B. J., McDowell J. C., 1994, ApJ, 435, 611

Loredo T. J., 1990, in Fougére P. F., ed., Maximum Entropy and Bayesian Methods. Kluwer, Dordrecht, p. 81

Maccacaro T., Gioia I. M., Wolter A., Zamorani G., Stocke J. T., 1988, ApJ, 326, 680

McHardy I. M. et al., 1999, MNRAS, 295, 641

Nandra K., Pounds K. A., 1992, Nat, 359, 215

Nandra K., Pounds K. A., 1994, MNRAS, 268, 405

Page M. J. et al., 1996, MNRAS, 281, 579

Pan H. C., Stewart G. C., Pounds K. A., 1990, MNRAS, 242, 177

Pounds K. A. et al., 1993, MNRAS, 260, 77

Press W. H., Teukolsky S. A., Vetterling W. T., Flannery B. P., 1992, Numerical Recipes. Cambridge Univ. Press, Cambridge, p. 617

Puchnarewicz E. M. et al., 1996, MNRAS, 281, 1243

Puchnarewicz E. M. et al., 1997, MNRAS, 291, 177

Raymond J. C., Smith B. W., 1977, ApJS, 35, 419

Reimers D., Bade N., Schartel N., Hagen H. J., Engels D., Toussaint F., 1995, A&A, 296, 49

Romero-Colmenero E., Branduardi-Raymont G., Carrera F. J., Jones L. R., Mason K. O., McHardy I. M., Mittaz J. P. D., 1996, MNRAS, 282, 94

Sarazin C. L., 1986, Reviews of Modern Physics, 58, 1

Schartel N., Walter R., Fink H. H., Trümper J., 1996, A&A, 307, 33

Schmitt J.H.M.M., Collura A., Sciortino S., Vaiana G. S., Harnden F. R., Rosner R., 1990, ApJ, 365, 704

Snowden S. L., McCammon D., Burrows D. N., Mendenhall J. A., 1994, ApJ, 424, 714

Stark A., Gammie C., Wilson R., Bally J., Linke R., Heiles C., Hurwitz M., 1992, ApJS, 79, 77

Thompson R. J., Cordova F. A., 1994, ApJ, 434, 54

Turner T. J., Pounds K. A., 1988, MNRAS, 232, 463

Vikhlinin A., Forman W., Jones C., Murray S., 1995, ApJ, 451, 564

Walter R., Fink H. H., 1993, A&A, 274, 105

This paper has been typeset from a TEX/LATEX file prepared by the author.